AD-A195 604 MODELING OF MICROMECHANISMS OF FATIGUE AND FRACTURE IN 1/1
HYBRID MATERIALS(U) CALIFORNIA UNIV BERKELEY DEPT OF
MATERIALS SCIENCE AND MINERA.. R O RITCHIE ET AL.
UNCLASSIFIED MAY 88 UCB/R/88/A1053 AFOSR-87-0158 F/G 11/4 NL

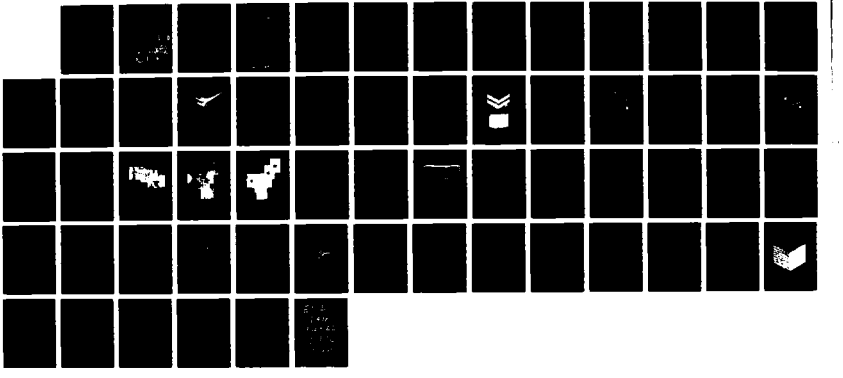

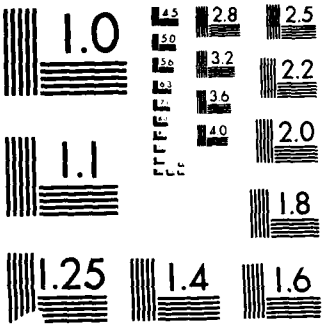


UTION TEST CHART

First Annual Report
to
U.S. Air Force Office of Scientific Research
on

# MODELING OF MICROMECHANISMS OF FATIGUE AND FRACTURE IN HYBRID MATERIALS

Grant AFOSR-87-0158
for period 15 April 1987 to 14 April 1988

by
R. O. Ritchie, W. Yu and S. C. Siu

May 1988

Report No. UCB/R/88/A1053



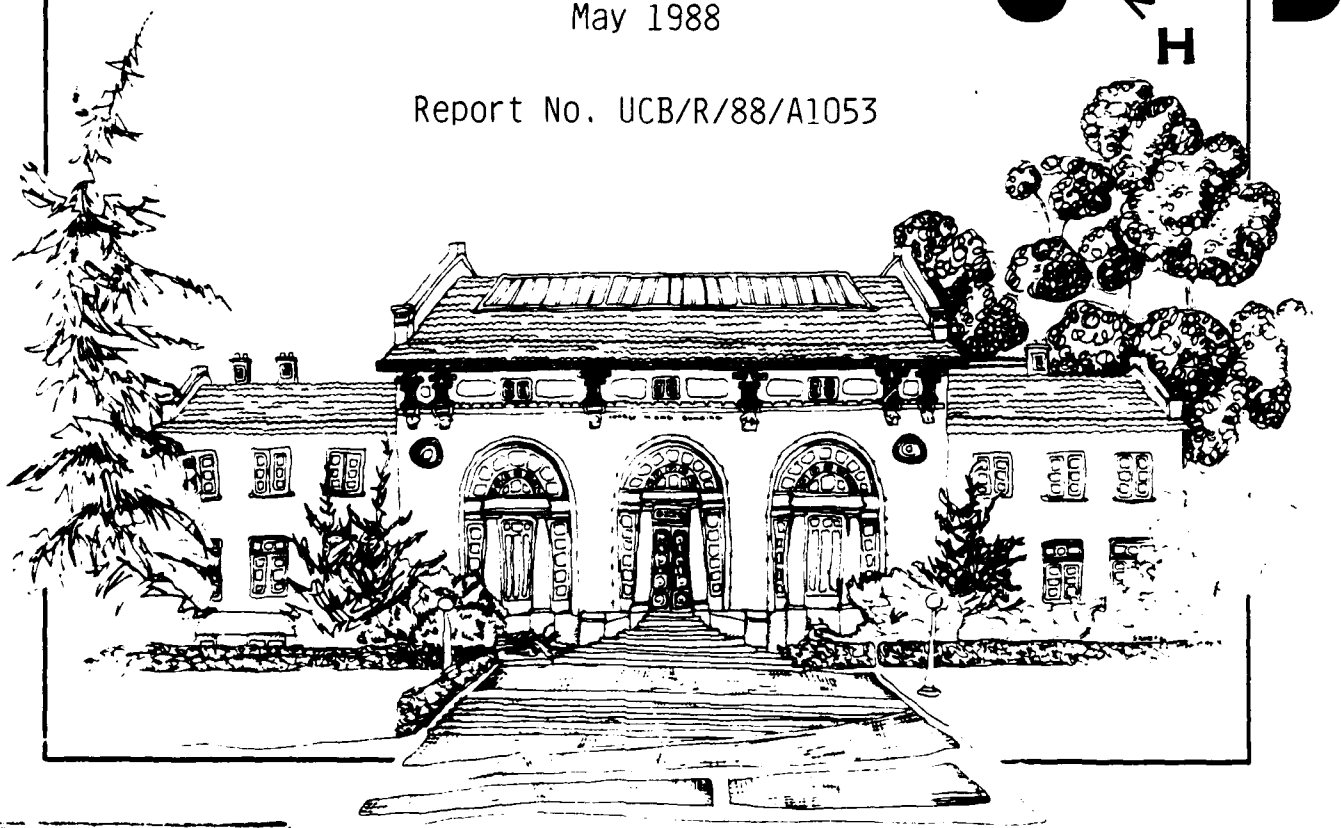



Department of Materials Science and Mineral Engineering
University of California, Berkeley, CA 94720

Report No. UCB/R/88/A1053

First Annual Report

to

U.S. Air Force Office of Scientific Research

on

# MODELING OF MICROMECHANISMS OF FATIGUE AND FRACTURE IN HYBRID MATERIALS

Grant No. AFOSR-87-0158

for period 15 April 1987 to 14 April 1988

submitted to

U.S. Air Force Office of Scientific Research
Bldg. 410, Bolling Air Force Base
Washington, D.C. 20322
Attention: Dr. Alan H. Rosenstein

submitted by

R. O. Ritchie, W. Yu and S. C. Siu
Department of Materials Science and Mineral Engineering
University of California
Berkeley, California 94720

May 1988

UNCLASSIFIED
SECURITY CLASSIFICATION OF THIS PAGE

# REPORT DOCUMENTATION PAGE

| | |
|---|---|
| 1a. REPORT SECURITY CLASSIFICATION<br>Unclassified | 1b. RESTRICTIVE MARKINGS<br>None |
| 2a. SECURITY CLASSIFICATION AUTHORITY<br>Not Applicable | 3. DISTRIBUTION/AVAILABILITY OF REPORT<br>Not Applicable |
| 2b. DECLASSIFICATION/DOWNGRADING SCHEDULE<br>Not Applicable | |
| 4. PERFORMING ORGANIZATION REPORT NUMBER(S)<br>UCB/R/88/A1053 | 5. MONITORING ORGANIZATION REPORT NUMBER(S)<br>AFOSR-TR- 88-0613 |
| 6a. NAME OF PERFORMING ORGANIZATION<br>Robert O. Ritchie, Dept. of Mat. Sci. & Minl. Eng. | 6b. OFFICE SYMBOL (If applicable) |
| 7a. NAME OF MONITORING ORGANIZATION<br>Air Force Office of Scientific Research AFOSR/NE | |
| 6c. ADDRESS (City, State, and ZIP Code)<br>University of California<br>Hearst Mining Building<br>Berkeley, California 94720 | 7b. ADDRESS (City, State, and ZIP Code)<br>Bldg. 410, Bolling AFB<br>Washington, D.C. 20322<br>ATTN: Dr. A. H. Rosenstein, AFOSR/NE |
| 8a. NAME OF FUNDING/SPONSORING ORGANIZATION<br>Same as 7a | 8b. OFFICE SYMBOL (If applicable) |
| 9. PROCUREMENT INSTRUMENT IDENTIFICATION NUMBER<br>AFOSR-87-0158 | |
| 8c. ADDRESS (City, State, and ZIP Code)<br>Same as 7b | 10. SOURCE OF FUNDING NUMBERS |

| PROGRAM ELEMENT NO. | PROJECT NO. | TASK NO. | WORK UNIT ACCESSION NO. |
|---|---|---|---|
| 61102F | 2306 | A1 | |

11. TITLE (Include Security Classification)
MODELING OF MICROMECHANISMS OF FATIGUE AND FRACTURE IN HYBRID MATERIALS (Unclassified)

12. PERSONAL AUTHOR(S)
RITCHIE, R. O., YU, W., and SIU, S. C.

| 13a. TYPE OF REPORT | 13b. TIME COVERED | 14. DATE OF REPORT (Year, Month, Day) | 15. PAGE COUNT |
|---|---|---|---|
| Annual | FROM 87/4/15 TO 88/4/14 | 1988 May 1 | |

16. SUPPLEMENTARY NOTATION

| 17. COSATI CODES | | |
|---|---|---|
| FIELD | GROUP | SUB-GROUP |
| | | |
| | | |

18. SUBJECT TERMS (Continue on reverse if necessary and identify by block number)
Fatigue; Fracture Toughness; Subcritical Crack Growth; Metal-Matrix Composites; Laminates; Fatigue Cracks: Crack Closure, Crack Bridging; Aluminum Alloys; Magnesium Alloys; Crack Propagation. (JES)

19. ABSTRACT (Continue on reverse if necessary and identify by block number)

The obvious benefits of the design of aerospace structures using lighter materials with high specific strengths and stiffnesses has led in recent years to the development of numerous reinforced composite materials, which have become serious commercial competitors to traditional monolithic metallic alloys. While significant advances in processing technology have made the fabrication of such hybrid materials more of an economic reality, their widespread use in airframes or other critical structures has in general been limited by serious deficiencies in particular mechanical properties, such as ductility, toughness and fatigue. This problem is often compounded by the lack of fundamental studies which provide a rational basis for the underlying sources of crack-propagation resistance in these materials, and in particular which define the critical role of composite microstructure. Accordingly, the current program is aimed at studying the physics and micromechanisms of fracture toughness and particularly the fatigue-crack growth resistance in laminate, discontinuously-reinforced and continuously-reinforced metal-matrix composites, with special reference to the role of microstructure. The central hypothesis of this work is that crack-propagation behavior in these materials primarily results from mutual competition between intrinsic toughening mechanisms, which increase the microstructural resistance to crack extension, and

| 20. DISTRIBUTION/AVAILABILITY OF ABSTRACT | 21. ABSTRACT SECURITY CLASSIFICATION |
|---|---|
| ☒ UNCLASSIFIED/UNLIMITED ☐ SAME AS RPT. ☐ DTIC USERS | Unclassified |
| 22a. NAME OF RESPONSIBLE INDIVIDUAL<br>~~Robert O. Ritchie~~ Rosenstein | 22b. TELEPHONE (Include Area Code)<br>~~769 4917~~ 767-4937 |
| | 22c. OFFICE SYMBOL<br>NE |

DD FORM 1473, 84 MAR 83 APR edition may be used until exhausted. All other editions are obsolete.

SECURITY CLASSIFICATION OF THIS PAGE
Unclassified

extrinsic mechanisms, which reduce the local "driving force" through crack-tip shielding. Current studies are focused on i) the role of crack deflection in influencing fatigue-crack growth behavior in aluminum alloys reinforced with sheets of epoxy impregnated with high-strength unidirectional aramid fibers (ARALL Laminates®), ii) long and microstructurally-small crack growth in cyclically-loaded aluminum alloys continuously-reinforced with unidirectional SiC fibers, and iii) the fatigue-crack growth behavior of graphite-reinforced magnesium alloy sheet. The highlight of the first year's work is the development of an experimental technique to provide, for the first time, a quantitative measure of the local crack-tip stress intensity in a hybrid material undergoing crack-bridging phenomena.

## TABLE OF CONTENTS

# MODELING OF MICROMECHANISMS OF FATIGUE AND FRACTURE IN HYBRID MATERIALS

R. O. Ritchie, W. Yu and S. C. Siu

(Grant No. AFOSR-87-0158)

## FORWARD

This manuscript constitutes the First Annual Report on Grant No. AFOSR-87-0158, administered by the U.S. Air Force Office of Scientific Research, with Dr. Alan H. Rosenstein as program manager. The work, covering the period April 15, 1987, through April 14, 1988, was performed under the direction of Dr. R. O. Ritchie, Professor of Materials Science, University of California in Berkeley, with Dr. W. Yu as Research Engineer, S. C. Siu as graduate student, and A. Nyguen as undergraduate engineering aide.

## ABSTRACT

The obvious benefits of the design of aerospace structures using lighter materials with high specific strengths and stiffnesses has led in recent years to the development of numerous reinforced composite materials, which have become serious commercial competitors to traditional monolithic metallic alloys. While significant advances in processing technology have made the fabrication of such hybrid materials more of an economic reality, their widespread use in airframes or other critical structures has in general been limited by serious deficiencies in particular mechanical properties, such as ductility, toughness and fatigue. This problem is often compounded by the lack of fundamental studies which provide a rational basis for the underlying sources of crack-propagation resistance in these materials, and in particular which define the critical role of composite microstructure. Accordingly, the current program is aimed at studying the physics and micromechanisms of fracture toughness and particularly the fatigue-crack growth resistance in laminate, discontinuously-reinforced and continuously-reinforced metal-matrix composites, with special reference to the role of microstructure. The central hypothesis of this work is that crack-propagation behavior in these materials primarily results from mutual competition between intrinsic toughening mechanisms, which increase the microstructural resistance to crack extension, and extrinsic mechanisms, which reduce the local "driving force" through crack-tip shielding. Current studies are focused on i) the role of crack

bridging and crack deflection in influencing fatigue-crack growth behavior in aluminum alloys reinforced with sheets of epoxy impregnated with high-strength unidirectional aramid fibers (ARALL Laminates®), ii) long and microstructurally-small crack growth in cyclically-loaded aluminum alloys continuously-reinforced with unidirectional SiC fibers, and iii) the fatigue-crack growth behavior of graphite-reinforced magnesium alloy sheet. The highlight of the first year's work is the development of an experimental technique to provide, for the first time, a quantitative measure of the local crack-tip stress intensity in a hybrid material undergoing crack-bridging phenomena.

# 1. INTRODUCTION

In recent years, the need for lighter materials with high specific strengths and stiffnesses, coupled with major advances in processing, has led to the development of numerous composite or hybrid materials as serious competitors to traditional engineering alloys. The majority of such materials are reinforced with high-strength, high-modulus (and often brittle) second phases, in the form of fibers, whiskers, particles or laminated sheets, embedded in a more ductile metallic or polymeric matrix, although other permutations such as ceramic-ceramic composites are not uncommon. Often, the properties of hybrid materials are highly anisotropic compared to equivalent monolithic materials, showing both distinct improvements and distinct detriments in specific mechanical properties.

Of particular interest in the aerospace and defense industry are polymer- or ceramic-reinforced metal-matrix composites [1]. Here, much effort has been directed towards the development of high performance composites utilizing aluminum and titanium matrices [2]. Where very high strengths and moduli are required for specialized applications, particularly at temperatures 100 degrees or so above that normally contemplated for the corresponding monolithic alloy, the use of aligned continuous fibers has been considered to induce very high, directional properties [3]. Conversely, for lower cost applications where such extreme properties are not a requirement, discontinuous metal-matrix composites consisting of whisker, nodule,

platelet or particulate reinforcement (e.g., typically involving up to 40 volume % of SiC) have been shown to offer substantially improved strength and modulus properties compared to conventional aluminum alloys [2-8]. In the latter case, the advantages of the discontinuous composites are that properties become essentially isotropic, and that fabrication can be achieved with standard metallurgical processing, such as powder metallurgy, direct casting, rolling, extrusion, etc. However, their disadvantage is poor ductility, toughness and fatigue-crack growth performance compared to that of the constituent matrix.

Where toughness and especially fatigue properties are a necessity, such as in tension-dominated, fatigue and fracture critical aircraft structures (e.g., fuselages, lower wings, tail skins), a third class of weight-sensitive metal-matrix composite, involving metal-organic polymer laminates, has shown particular promise [9-12]. Such hybrids, which consist of thin aluminum-alloy sheets bonded by adhesive impregnated with strong aramid fibers (ARALL Laminates®), show spectacular resistance to fatigue-crack growth without compromise in strength, and further retain all the traditional advantages of a metal, i.e., plasticity, impact strength, formability and machinability [12]. Whereas potential weight savings of between 15 and 30% have been projected for aircraft structures utilizing ARALL, the disadvantages of these materials are their

---

®ARALL Laminate is a registered trademark of the Aluminum Company of America.

current low resistance to shear or delamination, and their toughness or residual strength in the presence of a notch or through-thickness crack (in which the fibers are broken).

Despite the radical impact of the potential widespread use of metal-matrix composites in the aerospace industry, it is perhaps surprising that relatively few systematic studies of a fundamental nature have been performed to related mechanistically, and ultimately model, the role of the composite microstructure in controlling toughness and fatigue resistance in these materials. This is particularly important as crack-propagation resistance is often the limiting property. In fact, in a very recent review of SiC-reinforced aluminum alloy composites [2], it was concluded that fracture toughness was the least investigated aspect of their material behavior, and furthermore that "...the fracture science of (these) composites needs to be re-examined...". This lack of understanding is illustrated by the case of P/M aluminum alloys discontinuously reinforced with platelet SiC. These materials are relatively isotropic, light weight, high modulus, high strength materials with improved wear and creep resistance, which are economical to produce and easy to shape. However, with all these advantages, they have yet to be used for airframes or other critical structures, primarily because of their inadequate ductility and fracture toughness [5]. Clearly, the factors governing the toughness of composite microstructures are far more complex than in homogeneous materials. In fact, as stated by Harris, there is no simple recipe

to date for predicting the properties in all composites [13], as the viable mechanisms for impeding crack growth are both numerous and in many cases extremely material specific.

An example of the complexities of toughening hybrid materials can be appreciated by considering the role of the interface. It is clear that the extension of a crack will be affected by the presence of the interface, both at the microstructural level between the fiber and the matrix and at the macroscopic level as planes of weakness between separate laminations in a multiple laminate. However, it is by no means clear what the nature of the interface should be for optimum toughness. For most metal-matrix fiber composites, it is the perception that a strong interfacial bond is required between the matrix and fiber [2]. Many ceramic-ceramic composites, conversely, derive their best fracture resistance where the interfacial shear strength is weak, such that relative sliding along the interface permits the matrix crack to grow leaving the fibers intact and bridging the crack [14]. In fact, it is interesting to note that one of the few metal-matrix composites with excellent crack-growth resistance, namely ARALL Laminates, have a weak interface between the aramid fibers and epoxy matrix to permit controlled delamination and hence crack bridging by unbroken fibers [10].

Accordingly, the principal thesis of this study is to identify and model the salient micromechanisms of toughening and fatigue resistance in each of the three classes of metal-matrix hybrid materials (laminates, continuous fiber and discontinuously reinforced

composites), and specifically to relate these mechanisms to the characteristic features of the microstructure. The approach is considered to be novel in that it will employ, and optimize, the two distinct routes to achieve toughening in materials, namely intrinsic mechanisms, which enhance the material's resistance to crack advance, and extrinsic mechanisms, which locally reduce the "driving force" for such advance [15]. The ultimate aim of this work is to describe and model in quantitative fashion the mechanisms of failure of advanced hybrid materials on the microstructural scale, and to utilize this understanding to provide a basis for the rational design of new composite microstructures with improved fracture and fatigue properties.

This report covers the first year of the program of research where attention has been focused on quantification of crack-tip shielding behavior, specifically by crack bridging and crack closure, during fatigue-crack propagation behavior in ARALL Laminates. In addition, on-going research programs are described on the micromechanisms of fatigue-crack propagation in continuously-reinforced metal-matrix composites, specifically involving SiC-fiber-reinforced aluminum alloys and graphite-reinforced magnesium alloys.

## 1.1 References


1. S. Dermarkar, Metals and Materials, 2 (1986) p. 144.

2. S. V. Nair, J. K. Tien, and R. C. Bates, Int. Metals Rev., 30 (1985) p. 275.

3. D. L. McDanels, Metall. Trans. A, 16A (1985) p. 1105.

4. R. J. Arsenault, Mater. Sci. Eng., 64 (1984) p. 171.

5. Y. From and R. J. Arsenault, J. Metals, 38 (1986) p. 31.

6. W. A. Logsdon and P. K. Liaw, Eng. Fract. Mech., 24 (1986) p. 737.

7. D. R. Williams and M. E. Fine, in Fifth Intl. Conf. Composite Matls. (ICCM-V), W. C. Harrigan et al., eds., TMS-AIME, Warrendale, PA, 1985, p. 639.

8. D. L. Davidson, Metall. Trans. A, 18A (1987) p. 2215.

9. L. B. Vogelesang and J. W. Gunnink, "ARALL, a Material for the Next Generation of Aircraft. A State of Art," Report LR-400, Delft University of Technology, The Netherlands, 1983.

10. R. Marissen, Eng. Fract. Mech., 19 (1984) p. 261.

11. R. W. Schultz, M. A. Gregory, and J. L. Teply, in Proc. First OMAE Speciality Symp. on Offshore and Arctic Frontiers, M. M. Salama, ed., American Society of Mechanical Engineers, New York, NY, 1986.

12. R. J. Bucci, L. N. Mueller, R. W. Schultz, and J. L. Prohaska, "Results from a Cooperative Test Program on ARALL, Aramid Aluminum Laminate," ALCOA Report, Aluminum Company of America, Alcoa Center, PA, 1986.

13. B. Harris, Metal Science, 14 (1980) p. 351.

14. A. G. Evans, M. D. Thouless, D. P. Johnson-Walls, E. Y. Luh, and D. B. Marshall, in Proc. Fifth Int. Conf. on Composite Materials, (ICCM-V), W. C. Harrigan et al., eds., TMS-AIME, Warrendale, PA, 1985, p. 543.

15. R. O. Ritchie, Mater. Sci. Eng. (1988) in press.

# 2. MEASUREMENT OF THE EFFECT OF CRACK-TIP SHIELDING FROM CRACK BRIDGING DURING FATIGUE-CRACK GROWTH IN ARALL LAMINATES

## 2.1 Introduction

Aramid-fiber reinforced aluminum-alloy laminates (ARALL® LAMINATE) are a new class of hybrid materials which consist of alternating layers of thin aluminum-alloy sheets bonded by a structural metal adhesive impregnated with high-strength unidirectional aramid fibers (Fig. 2.1). Originally developed for fatigue-critical aircraft structures where up to 50% potential weight savings has been predicted [1-4], these composites show a range of attractive, albeit directional, properties, including 15-20% lower density, up to 60% higher strength (at comparable stiffness), good impact and damping properties, and most importantly superior fatigue crack propagation resistance, compared to monolithic high-strength aluminum alloys [1-5]. Moreover, property characteristics can be readily modified, for example, through the use of post-stretching or by using various matrix alloys, varying fiber-resin systems, and different stacking sequences and cross-plies, although few of these variants are commercially available at present.

ARALL derives its superior crack-growth properties (under tensile loading) by promoting extensive crack bridging in the wake of the crack tip [4-8]. Mechanistically, for crack extension perpendicular to the fiber direction, as the crack propagates in the aluminum layers, controlled delamination between the metal, epoxy and

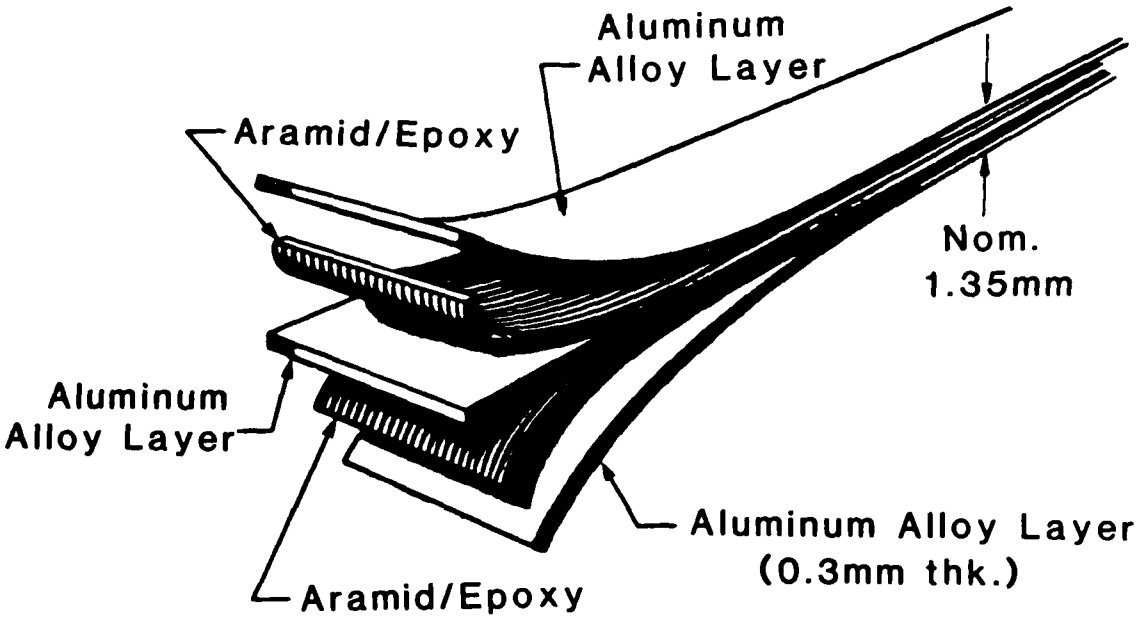


Schematic of ARALL Laminate

Fig. 2.1: Illustration of the layup of 3/2 ARALL-2 Laminate.

fiber interfaces redistributes stresses both ahead and behind the tip, permitting individual aramid fibers to remain intact and span the crack in the wake of the tip [7,8]. Thus, similar to behavior in certain ceramic-matrix composites [9], the fibers act as bridges to restrain crack opening, thereby reducing the effective "crack driving force" actually experienced at the crack tip. In stretched ARALL Laminates, where the metal layers are left in residual compression and the fibers in residual tension, self-arrest can result with crack extension [10], leading to the claim that ARALL is a "fatigue insensitive" material.

Crack bridging in ARALL Laminates is an example of crack-tip shielding, where toughness is enhanced, or more generally crack advance is impeded, not by increasing the intrinsic microstructural resistance but by mechanisms which act to lower the local near-tip "driving force" [11,12]. As illustrated schematically in Fig. 2.2 [11,12], other examples include rubber-toughening in polymers [13], transformation, microcrack and fiber toughening in ceramics [14,15], crack bridging via uncracked ligaments in metals, ceramics and composites [16-18], and crack closure in fatigue [12,19]. In all these cases, the predominant shielding mechanisms act in the crack wake such that, depending upon the extent of the "shielding zone" behind the tip, crack-growth behavior becomes crack-size dependent, i.e., in terms of the globally calculated applied stress intensity K, the usually assumed similitude of the crack-tip fields for cracks of differing size will be compromised. This leads to certain

## EXTRINSIC TOUGHENING MECHANISMS

1. CRACK DEFLECTION AND MEANDERING

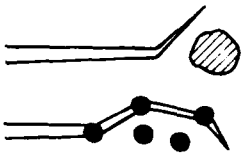

2. ZONE SHIELDING

— transformation toughening

— microcrack toughening

— crack wake plasticity

— crack field void formation

— residual stress fields

— crack tip dislocation shielding

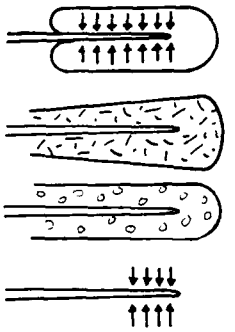

3. CONTACT SHIELDING

— wedging:

corrosion debris-induced crack closure

crack surface roughness-induced closure

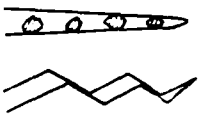

— bridging:

ligament or fiber toughening

— sliding:

sliding crack surface interference

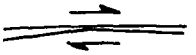

— wedging + bridging:

fluid pressure-induced crack closure

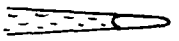

4. COMBINED ZONE AND CONTACT SHIELDING

— plasticity-induced crack closure

— phase transformation-induced closure

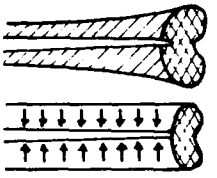

Fig. 2.2: Schematic representation of the classes and mechanisms of crack-tip shielding [11,12].

definitive fracture properties, such as marked resistance-curve toughness behavior, as seen for example in toughened ceramics [14,15,17], and the elevated growth rates of small cracks, as seen for near-threshold fatigue in metals [11,20,21].

The theoretical modelling of crack-tip shielding is in many cases well developed, particularly for the transformation/microcrack toughening [14,15,22] and crack-bridging mechanisms [7-9,16,17]. There have been few studies, however, to verify experimentally these models and specifically to measure the extent of shielding and the effective near-tip "driving force". An exception to this is crack closure in fatigue where an effective stress-intensity range can be evaluated, for example, in terms of compliance changes resulting from physical contact between the crack surfaces during the unloading cycle [e.g., refs. 11,23,24]. The primary objective of the present work is to describe experimental techniques to measure quantitatively the magnitude of crack-tip shielding by crack bridging as well as crack closure in an ARALL Laminate, in order to estimate the effective near-tip stress-intensity range during fatigue crack growth in this material. In addition, the mechanistic characteristics of crack propagation, delamination and crack-bridging behavior in the laminate are described for a wide spectrum of growth rates.

## 2.2 Experimental Procedures

**Materials:** The ARALL Laminate used in this study was a 1.35-mm-thick five-layer composite with two 0.2-mm-thick unidirectional

aramid-fiber/epoxy ("prepreg") layers sandwiched between three 0.3-mm-thick chromic-acid-anodized and primed 2024-T3 aluminum-alloy sheets, supplied and designated by Alcoa as a 3/2 ARALL-2 Laminate. The prepreg layers consist of an epoxy based adhesive system impregnated with uniaxial, high-modulus aramid fibers, in a 50/50 fiber/adhesive weight ratio. The fiber direction is aligned parallel to the rolling direction of the aluminum sheet. Curing is achieved at 121°C (with no subsequent stretch) [25]. The density of the resulting material is 2.29 g/cm$^3$, 18% lower than 2024. For comparative purposes, ARALL-2 Laminate behavior is compared to its 2024-T351 monolithic alloy counterpart.

**Microstructure and Mechanical Properties:** The microstructure of the laminate, including an enlarged view of the prepreg layer, is shown in Fig. 2.3. It is apparent that the fibers are not distributed evenly throughout the adhesive layer; resin-rich (i.e., fiber-poor) regions exist near the prepreg/metal interface [7]. Typical mechanical properties for the longitudinal (0°, loading parallel to fiber direction) and transverse (90°, loading perpendicular to fiber direction) orientations are compared to monolithic 2024-T3 (1.6-mm thick sheet) in Table 2.1 [25,26].

**Fatigue Testing:** Fatigue crack propagation tests on ARALL-2 Laminates were performed with compact C(T) test pieces, machined to a width of 50 mm from the full thickness of the plate in the L-T (0°,

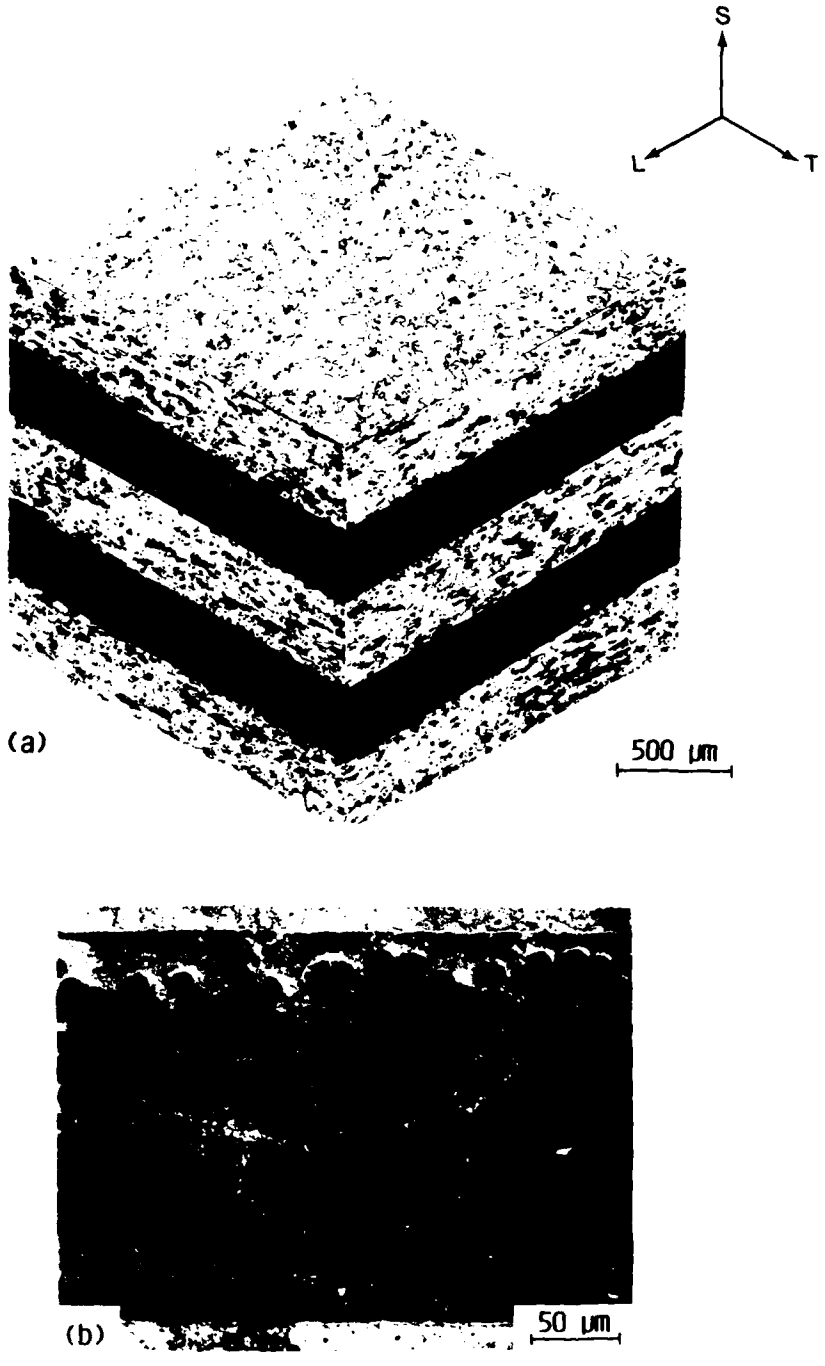


Fig. 2.3: Optical micrographs of a) three-dimensional microstructure of ARALL-2, and b) cross-section showing prepreg layers sandwiched between aluminum layers. Note in b) the resin-rich (fiber-poor) regions close to the prepreg/aluminum interfaces.

**Table 2.1 Typical Mechanical Properties of 3/2 ARALL-2 Laminate and 2024-T3**

| Average Mechanical Property | 3/2 ARALL-2 Laminate L (0°) | 3/2 ARALL-2 Laminate T (90°) | Monolithic 2024-T3 L | Monolithic 2024-T3 T |
|---|---|---|---|---|
| Tensile Modulus of Elasticity (GPa) | 64.1 | 49.0 | 72.4 | 72.4 |
| Ultimate Tensile Strength (MPa) | 717 | 317 | 455 | 448 |
| Tensile Yield Strength (MPa) | 359 | 228 | 359 | 324 |
| Compressive Yield Strength (MPa) | 262 | 234 | 304 | 345 |
| Tensile Total Strain to Failure (%) | 2.5 | 12.7 | 19.0 | 19.0 |

crack growth perpendicular to fiber direction) and T-L (90°, crack growth parallel to fiber direction) orientations. Comparison tests on 2024-T351 were performed on 7-mm-thick C(T) test pieces, machined in the T-L orientation from the center thickness of 25-mm-thick plate. All testing was carried out in controlled room-temperature air (22°C, 45% relative humidity) using a computer-controlled electro-servo-hydraulic testing machine, operating at 50 Hz sinsoidal frequency with a load ratio ($R = K_{min}/K_{max}$) of 0.1.

Crack lengths were monitored using a direct-current electrical-potential technique on the outer aluminum layer (Fig. 2.4). The accuracy of this technique in thin sheet was estimated to be within ± 0.01 mm on crack length. Additionally, the compliance of the

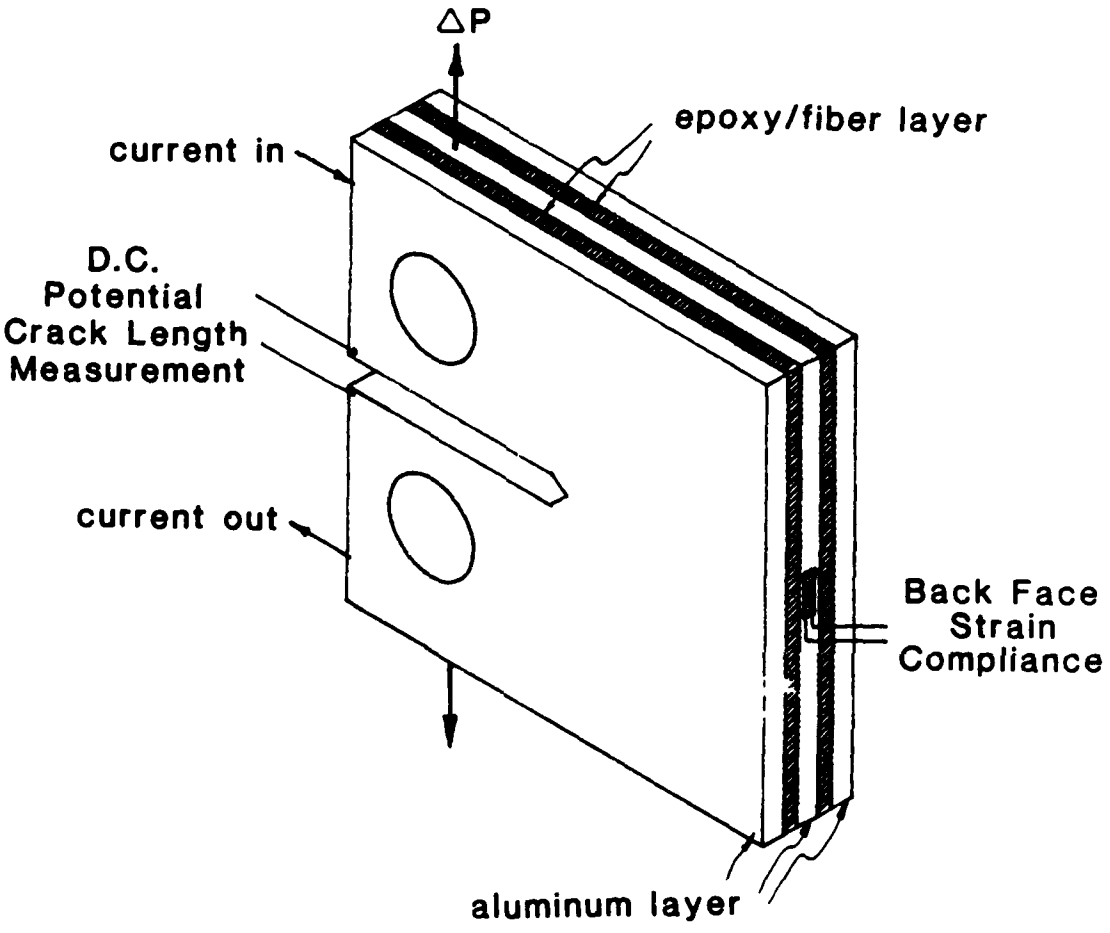


Fig. 2.4: Illustration of the fatigue test specimen showing the location of the electrical-potential crack monitoring probes, attached to the outer aluminum alyer, and the back-face strain gauge used to measure compliance, attached to the central aluminum layer.

specimen was monitored using a back-face strain gauge mounted on the central aluminum layer at the midpoint opposite the crack mouth (Fig. 2.4). Both electrical-potential and back-face strain signals were fed into a real-time computerized data-acquisition and control system, which was used both to control the test and to compute continuously compliance and crack-closure loads (see below). Stress intensities were calculated from standard handbook solutions [27] for the compact geometry, using the full thickness of the composite (unless otherwise stated).

The crack propagation tests were performed under computer control with a constant stress-intensity gradient, in general accordance with ASTM Standard E 647-86A. Data were first generated under decreasing $\Delta K$ conditions using an automated load-shedding scheme of $\Delta K = \Delta K_0 \exp[C^*(a - a_0)]$, where $\Delta K$ and $a$ are the instantaneous values of stress-intensity range ($K_{max} - K_{min}$) and crack length, $\Delta K_0$ and $a_0$ are their initial values, and $C^*$ is the normalized stress-intensity gradient set to -0.1 per mm of crack extension. Following crack arrest at a "threshold" condition, tests were continued under increasing $\Delta K$ conditions, with $C^*$ set to 0.15 $mm^{-1}$. Using these procedures, crack propagation rate data were generated over a wide spectrum of growth rates, from roughly $10^{-11}$ to $10^{-5}$ m/cycle.

## 2.3 Results and Discussion

**Fatigue Crack Growth Behavior:** Results of the constant-amplitude fatigue crack propagation tests, in the form of growth rates, da/dN, as a function of the nominal stress-intensity range, $\Delta K$, are shown in Fig. 2.5 for the 0° (L-T) and 90° (T-L) orientations in ARALL-2 Laminate; data are compared to that for monolithic 2024-T351 (T-L orientation).

Where fatigue crack propagation in the laminate is along the fiber direction (90° orientation), growth rates are faster than in the monolithic alloy, although the form of the growth-rate curve is similar. If the ARALL data for this orientation are normalized with respect to the actual total thickness of the aluminum in the composite, i.e., assume that the aluminum carries all load, crack growth rates for ARALL-2 (90°) coincide with those for the monolithic 2024-T351 alloy (Fig. 2.6). This result implies that the role of the fibers (and the resin) in the laminate can be ignored for crack growth in the transverse (90°) direction.

Conversely, where fatigue crack propagation in the laminate is perpendicular to the fiber direction (0° orientation), due to the contribution of the aramid fibers, behavior is quite different from 2024-T351. Firstly, growth rates in the laminate are in general significantly slower (by up to almost three orders of magnitude) than in the monolithic aluminum alloy, indicating that the fatigue crack growth resistance of ARALL-2 in this orientation is extremely high. Secondly, similar to behavior reported for other ARALL laminates

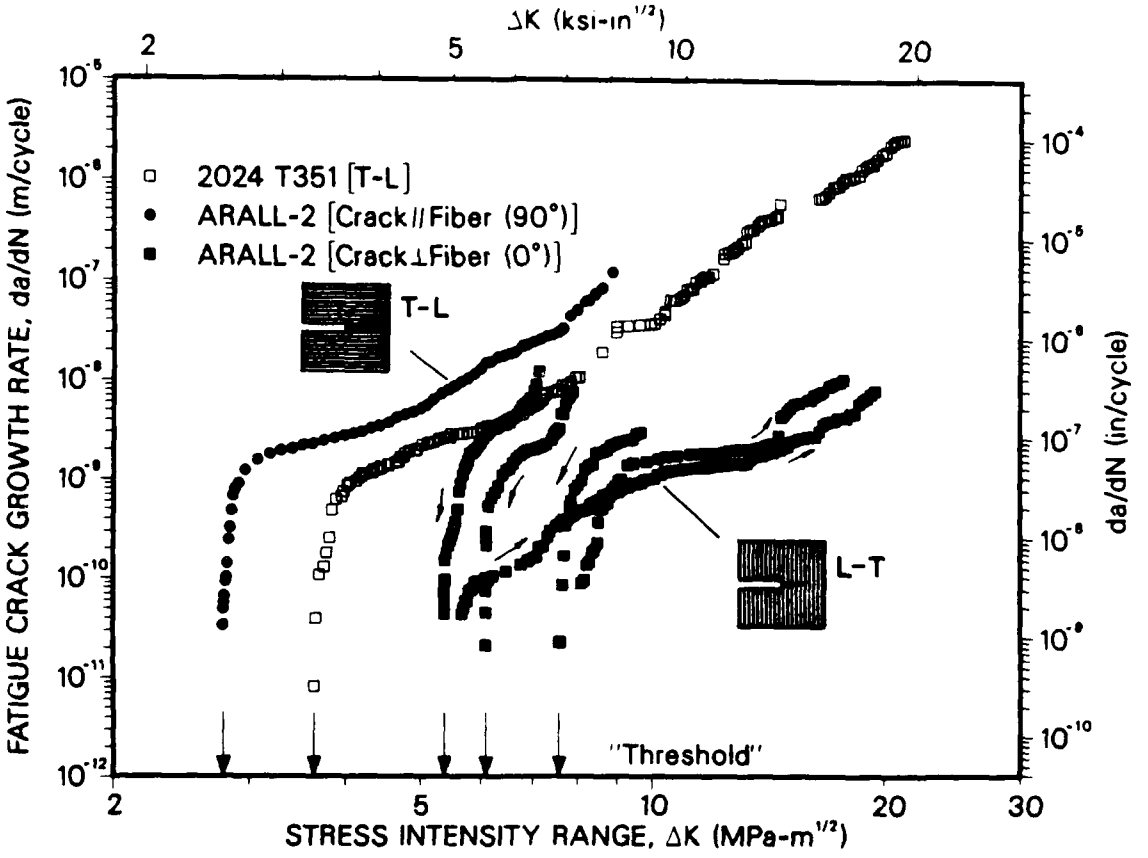


Fig. 2.5: Variation in fatigue crack propagation rates (da/dN) for ARALL-2 Laminate, as a function of the nominal stress-intensity range ($\Delta K = K_{max} - K_{min}$), in the longitudinal (0°, L-T) and transverse (90°, T-L) orientations. Data are compared with results for monolithic 2024-T351 alloy (T-L orientation). Vertical arrows show the effective fatigue "thresholds", i.e., the values of $\Delta K$ at crack arrest. Small arrows on curves indicate whether data were obtained under decreasing or increasing growth-rate conditions.

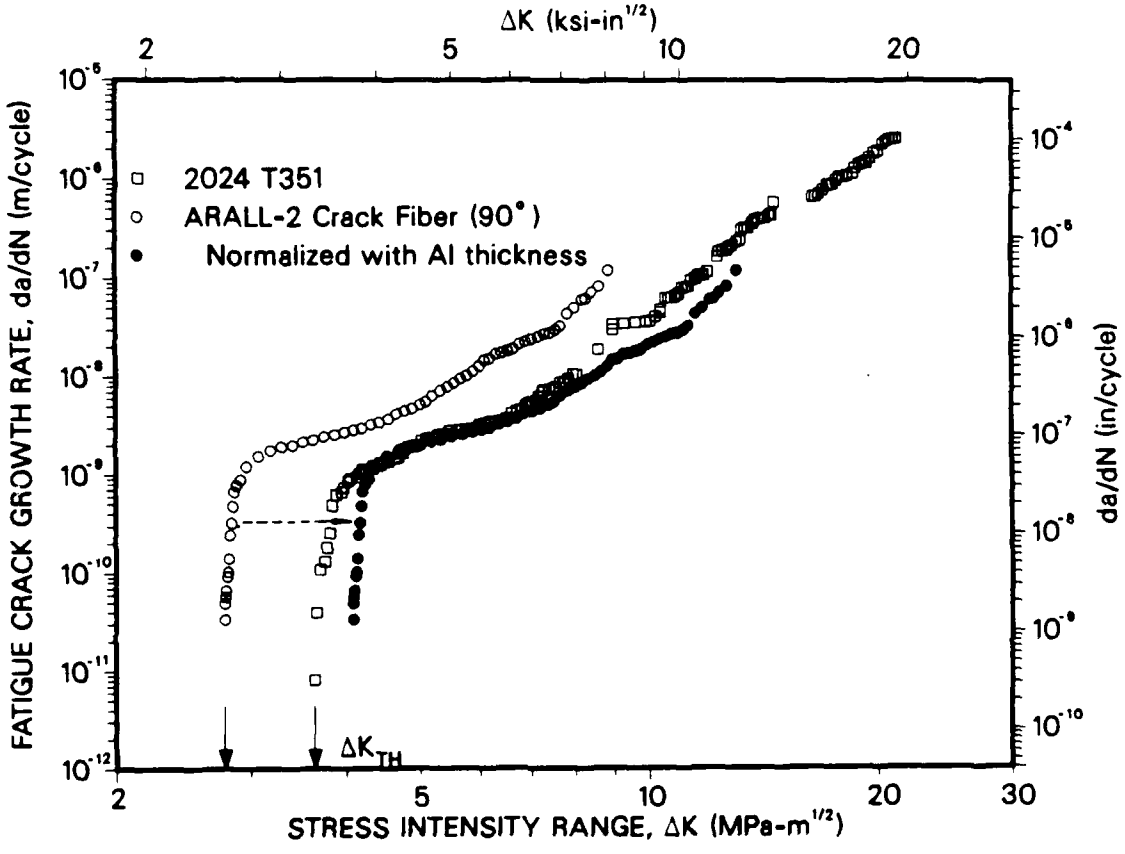


Fig. 2.6: Variation in fatigue crack propagation rates (da/dN) as a function of the nominal stress-intensity range (ΔK) for ARALL-2 and 2024-T351 alloy in the transverse (T-L) orientation, showing the correspondence of growth-rate behavior in the laminate and the monolithic alloy by assuming that the aluminum alyers carry all the load in ARALL-2.

[1-8,10,28], crack growth rates become non-unique with respect to the nominal stress-intensity range $\Delta K$, showing a marked history and crack-size dependence.

**Fractographic Studies:** The reinforcement role of the fibers during crack growth in the latter longitudinal (0°) orientation was examined using scanning electron microscopy of metallographic sections taken across the crack perpendicular to the crack surface. Figure 2.7 shows one such cross-section, located $\sim$ 3 mm from the crack tip, looking into the crack in the crack propagation direction, i.e., from the wake toward the tip. The fatigue crack can be readily seen in the aluminum layers, but is also still visible in the epoxy layer. Numerous strands of aramid fibers, however, remain unbroken across the crack.

To lower the probability of fiber breakage necessary to permit such crack bridging, some degree of controlled delamination is essential to reduce the magnitude of fiber loading and lower through-thickness constraint [8]. Claims that such delamination occurs principally within the epoxy near the prepreg/metal interface, specifically at the boundary between the fiber-rich and resin-rich layers [6-8], have been made. However, the fact that the crack can be imaged throughout the thickness of the epoxy layer (Figs. 2.7 and 2.8) suggests an alternative explanation. In the present case, the interface between the aluminum sheet and the epoxy, and between the resin-rich and fiber-rich layers within the epoxy, only suffered

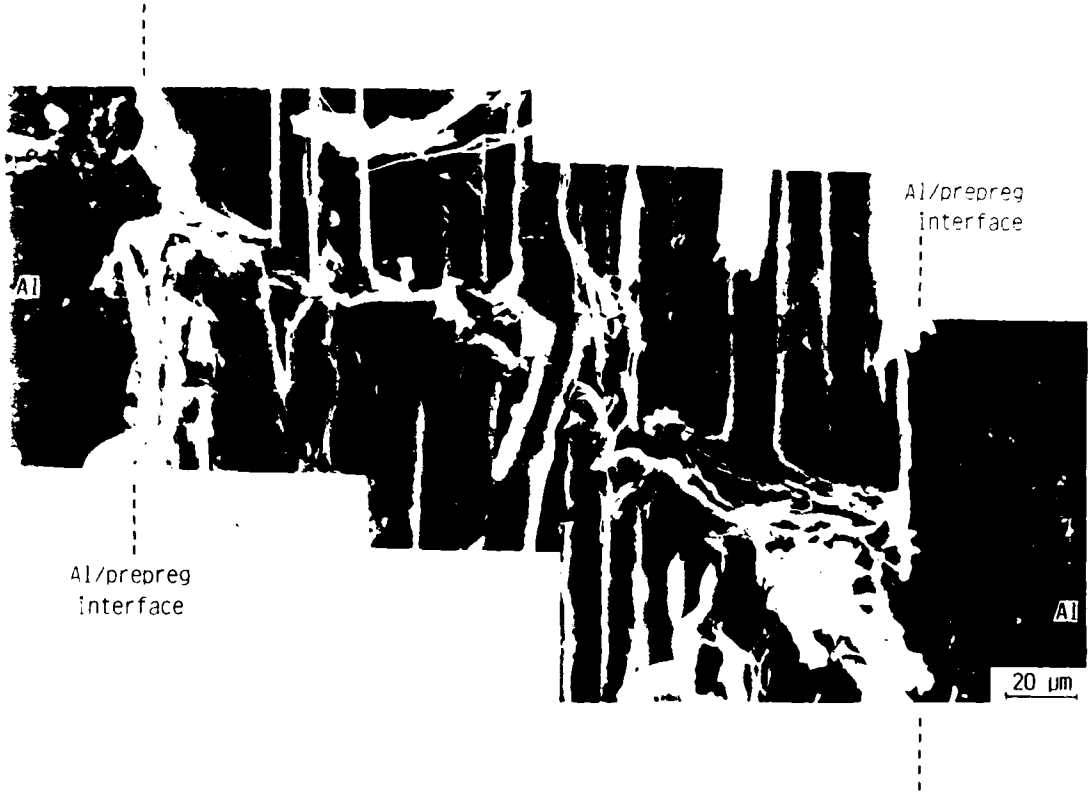


Fig. 2.7: Scanning electron micrograph of a metallographic section taken across the wake of a fatigue crack in ARALL-2 (imaged ∿3 mm from the crack tip, looking into the crack mouth toward the tip), showing numerous strands of unbroken aramid fibers bridging the crack. Note that the crack is still visible in the epoxy layer, indicating that the delamination is primarily at individual fiber/epoxy interfaces.

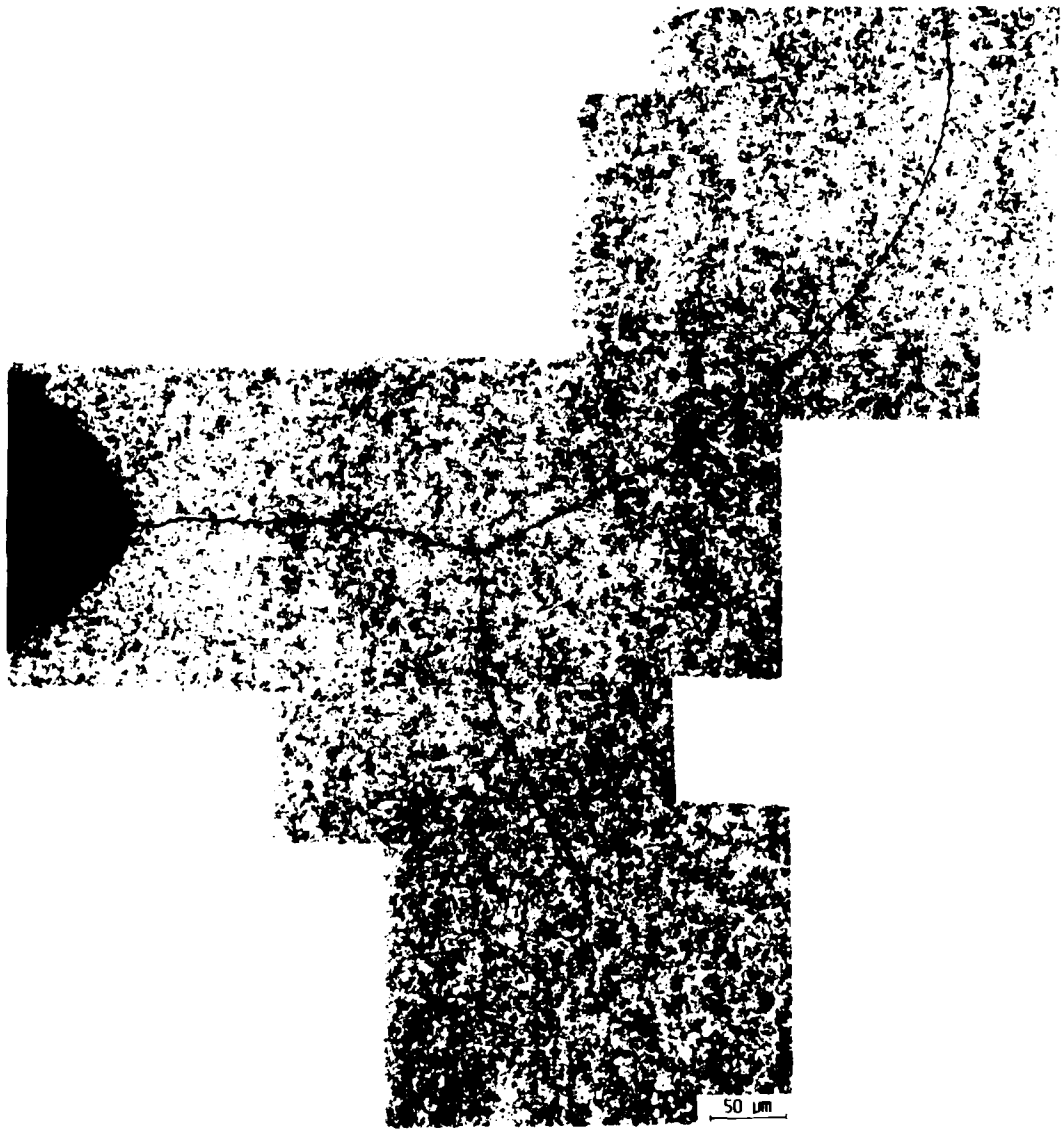


(a)

Fig. 2.8: Metallographic section perpendicular to the crack plane showing crack bifurcation during fatigue crack propagation at high stress-intensity ranges ($\Delta K \sim 15$ MPa$\sqrt{m}$) in ARALL-2, as imaged a) in the outer aluminum layer, and b) in the epoxy layer after etching away the aluminum. Note that as the crack is still visible within the epoxy layer, the principal delamination is not at the resin-rich/fiber-rich boundary.

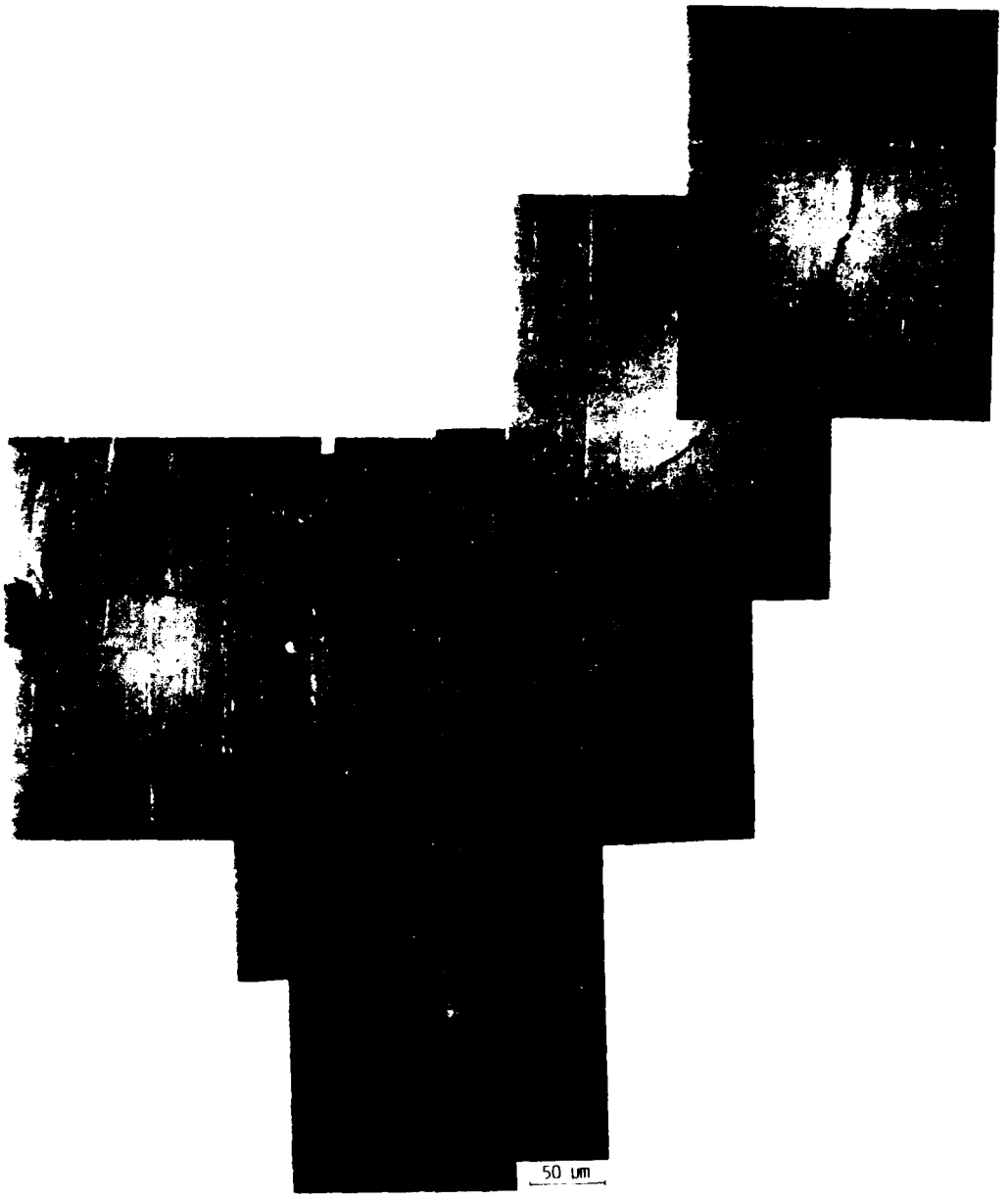


(b)

Fig. 2.8 (Cont.)

minor delamination, whereas extensive separation was apparent among various bundles of fibers, implying that failure of individual fiber/epoxy interfaces is the primary source of the delamination process.

Figure 2.7 also shows evidence of "bulged out" fibers at the crack line, which suggests some degree of prior kinking. Fiber kinking is known to be severely detrimental to the fatigue properties of ARALL as it promotes breakage of the aramid fibers [28]; for this reason ARALL laminates are intended for tension-dominated cyclic loading application, and as such are not suited for high compressive loading during service. However, such kinking in the present study is probably the result of the predominantly bending stress field implicit with compact test piece which, unlike center-cracked tension geometries, subjects fibers located well ahead of the crack tip (below the neutral axis) to prior compressive loads. Crack growth behavior in ARALL is thus predicted to be geometry-dependent.

Another example of geometry-dependent behavior is apparent at high stress-intensity ranges, where the marked difference in crack propagation resistance between the 0° and 90° orientations (due to selective fiber bridging) leads to a tendency for crack growth in the 0° direction to deviate along the fiber direction in compact C(T) geometries. This phenomenon causes marked crack bifurcation, as shown in Fig. 2.8, which results in additional crack-tip shielding by crack deflection at high $\Delta K$. However, in center-cracked tension

CC(T) sheet geometries, where off-angle crack propagation is not stabilized, such crack-bifurcation behavior is rarely observed.

**Measurement of Crack-Bridging Zone:** In order to verify further the role of fiber bridging influencing fatigue crack propagation behavior in ARALL, and specifically to determine the location and size of the "bridging zone" of unbroken fibers behind the crack tip (Fig. 2.9), experiments were performed where the wake of the crack was progressively removed while simultaneously monitoring the change in elastic compliance (as a measure of how much the fibers restrain crack opening).

The experiment was conducted on an arrested crack that had been cycled for $10^7$ cycles at an apparent threshold of $\Delta K = 7.6$ MPa$\sqrt{m}$, following normal load-shedding procedures. Using a fine jeweler's saw, a 1-mm-wide slot was machined from the V-notch along the dormant crack to within $\sim$ 0.2 mm of the crack tip. Approximately every 1 mm, the elastic compliance was measured using the back-face strain gauge mounted on the central aluminum layer (Fig. 2.4), while monitoring the length ($\tilde{a}$) of the remaining portion of the crack with a travelling microscope; results are plotted in Fig. 2.10a. For the $\sim$ 26-mm-long crack, removing the wake to within roughly 5 mm of the crack tip had little effect on the compliance, implying that the fibers were broken this far from the tip. Conversely, the compliance increased sharply as the last $\sim$ 5 mm of wake were removed, indicating

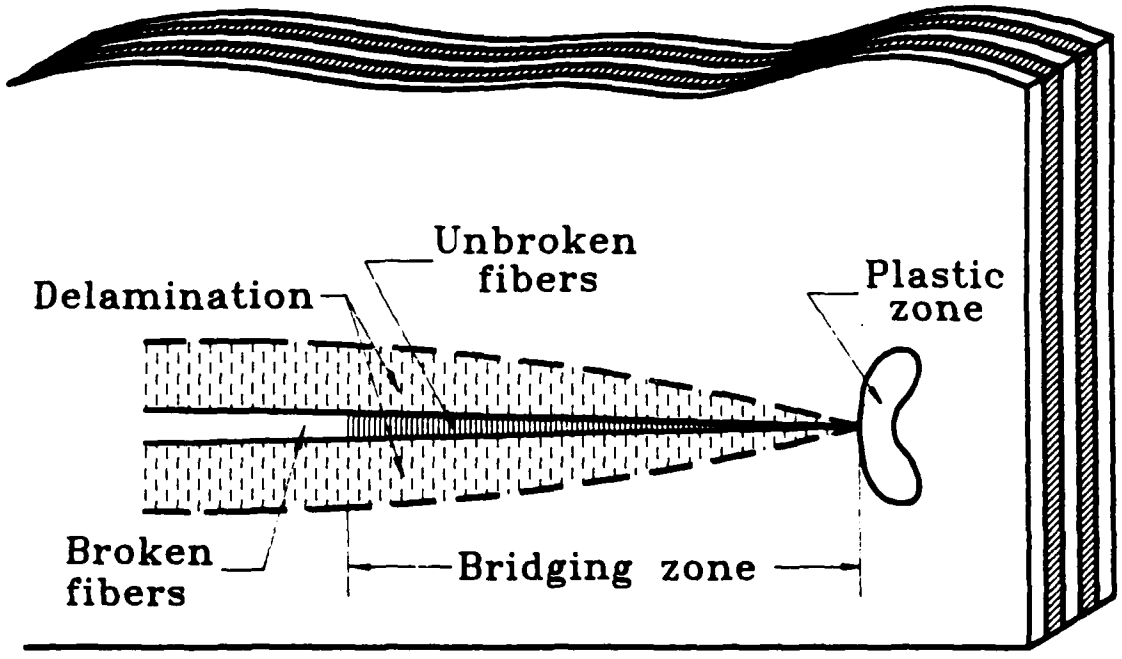


Fig. 2.9: Schematic illustration of a fatigue crack in ARALL, showing the location of the bridging (or shielding) zone.

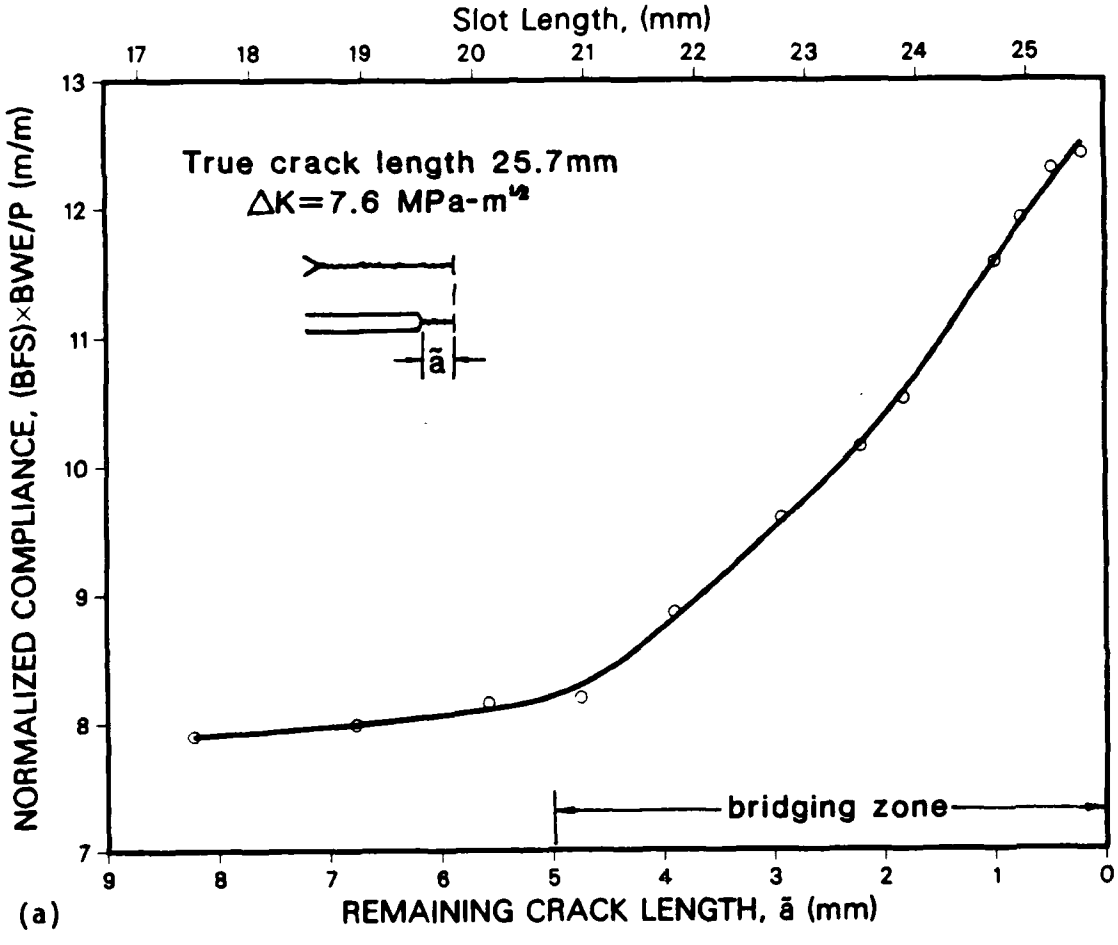


Fig. 2.10: Results of experiments to estimate the size of the bridging zone in ARALL showing a) the change in compliance as a function of the remaining length of fatigue crack, $\tilde{a}$, during progressive removal of the crack wake, and b) the initial acceleration and subsequent progressive deceleration of crack growth from the machined slot (initial $\tilde{a}$ = 0.2 mm). All results were determined at a constant $\Delta K$ of 7.6 MPa$\sqrt{m}$, where prior to machining the crack had arrested.

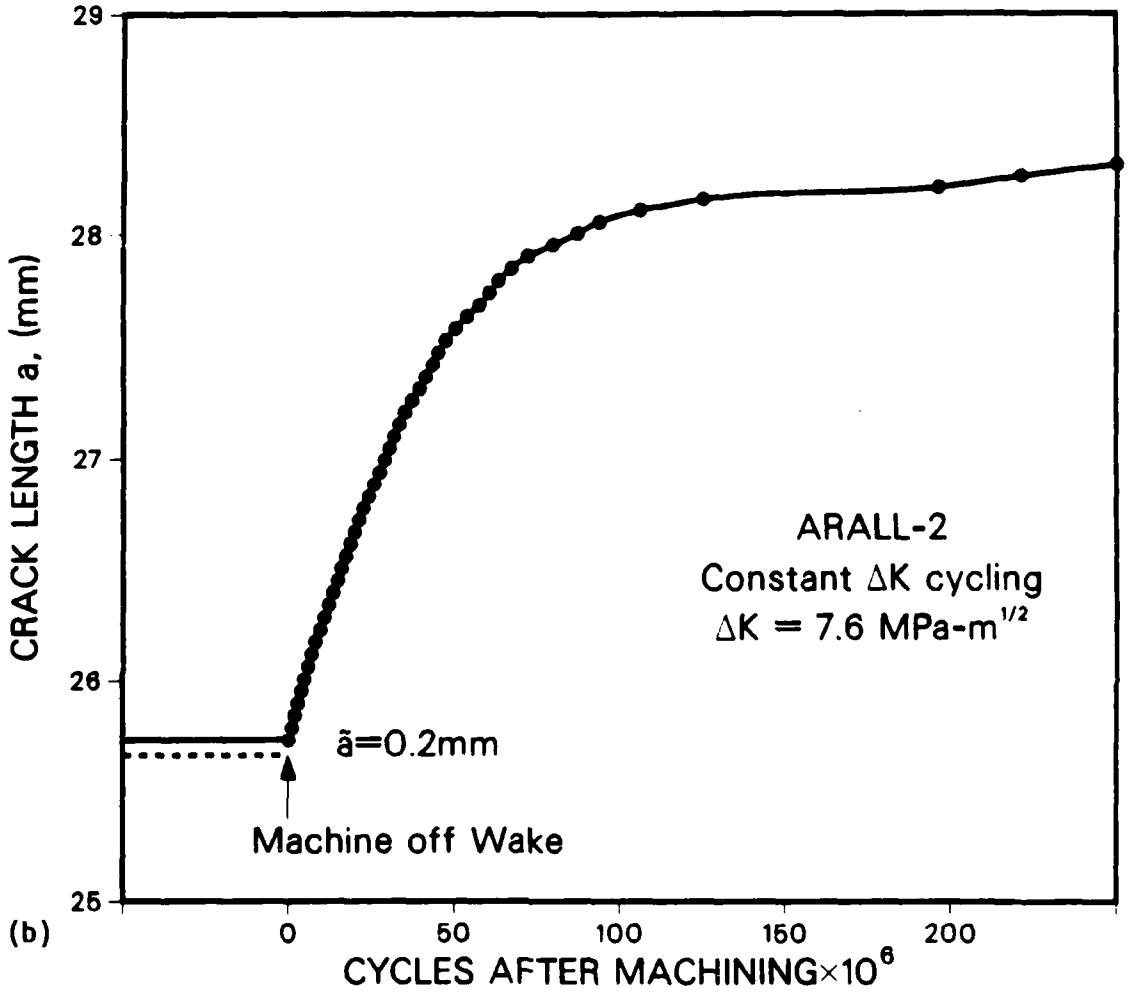
29
28
27
26
25
CRACK LENGTH a, (mm)
ARALL-2
Constant ΔK cycling
ΔK = 7.6 MPa-m^1/2
ã=0.2mm
Machine off Wake
(b)
0
50
100
150
200
CYCLES AFTER MACHINING×10^6

Fig. 2.10 (Cont.)

that the fibers in this region were originally intact across the fatigue crack and were being severed by the jeweller's saw.

Such measurements suggest a shielding (or bridging) zone in ARALL of the order of 5 mm behind the crack tip where the principal fiber bridging takes place. Compared to the size of this zone for other mechanisms of shielding in Fig. 2.2, this is extremely large. For example, similar wake-machining experiments in monolithic aluminum alloys to determine the extent of crack closure (primarily from asperity wedging) in the wake of a arrested cracks suggest shielding-zone sizes closer to 500 μm [29,30]. Furthermore, in the case of corrosion-debris induced crack closure, where the fretting oxide deposits accumulate only very close to the tip [31,32], the shielding zone may be less than ∿10 μm. Since the magnitude of the shielding zone behind the crack tip primarily dictates the history- and crack-size dependence of the crack-growth behavior, such results are consistent with the experimental observations (Fig. 2.5) that longitudinal growth rates in ARALL do not display a unique dependence upon $\Delta K$.

To examine the re-generation of the bridging zone with crack extension, following wake machining the remaining 0.2-mm fatigue crack, emanating from the machined slot, was cycled at the original "threshold" $\Delta K$ level of 7.6 MPa$\sqrt{m}$. As shown in Fig. 2.10b, although the crack commenced to propagate immediately on application of the cyclic load, growth rates progressively decayed with subsequent crack extension (at constant $\Delta K$) until the crack re-arrested after more

than $10^8$ cycles. The crack length needed for re-arrest, i.e., to re-establish a bridging zone behind the crack tip, can be seen to be of order of 3 mm, somewhat less than the 5 mm or so required for arrest during load shedding (Fig. 2.10a). Such differences presumably reflect different loading histories prior to arrest, namely decreasing $\Delta K$ conditions during programmed load shedding compared to constant $\Delta K$ conditions (at the lowest "threshold" level) in the above experiment.

**Measurement of Crack-Tip Shielding:** Whereas the fatigue crack propagation properties of ARALL Laminates in the longitudinal (0°) orientation are clearly excellent, from the perspective of analysis and prediction of crack extension and lifetime, the non-uniqueness of the crack growth data (in terms of $\Delta K$) is far from ideal. As noted above, such non-uniqueness, with respect to crack size, geometry and loading history, results from differing degrees of crack bridging in the wake of the crack (and associated delamination), which reduces the effective $\Delta K$ experienced locally at the crack tip. Although modelled by Marissen [7,8] for the center-cracked tension geometry, there have been no attempts experimentally to measure the bridging effect, in order to determine an effective $\Delta K$ which would suitably characterize the crack-tip fields in ARALL and thus potentially normalize the longitudinal crack growth data. Below we describe an experimental scheme, intended to provide this characterization through the measurement of the effect of crack-tip shielding from

both crack bridging and crack closure using combined electrical-potential and compliance monitoring.

**Principle:** The principle of the measurement technique is illustrated schematically in Fig. 2.11. Shielding is assumed to affect the applied "crack driving force", $\Delta K = K_{max} - K_{min}$, in two ways, specifically by crack closure (i.e., wedging through crack-surface contact), which primarily increases the effective $K_{min}$, and crack bridging, which primarily decreases the effective $K_{max}$.* Accordingly, the effective stress-intensity experienced at the tip may be defined as:

$$\Delta K_{eff} = K_{br} - K_{cl} \quad , \tag{2.1}$$

where $K_{br}$ is the effective $K_{max}$ (corrected for crack bridging) and $K_{cl}$ is the effective $K_{min}$ (corrected for crack closure). Experimental techniques to measure each parameter are described below.

**Crack closure:** In aluminum alloys at low $\Delta K$ levels, the principal source of crack closure arises from wedging of crack surfaces by

*It should be noted here that in the general case, crack closure, induced by cyclic plasticity [23] or fluid pressure [33] for example, may have a small additional influence in reducing the effective $K_{max}$. By the same token, depending upon the mechanical properties of the fibers, crack bridging may influence the effective $K_{min}$. However, the proposed measurements are not specific to the microstructural origins of the shielding mechanisms and will thus evaluate the total effect.

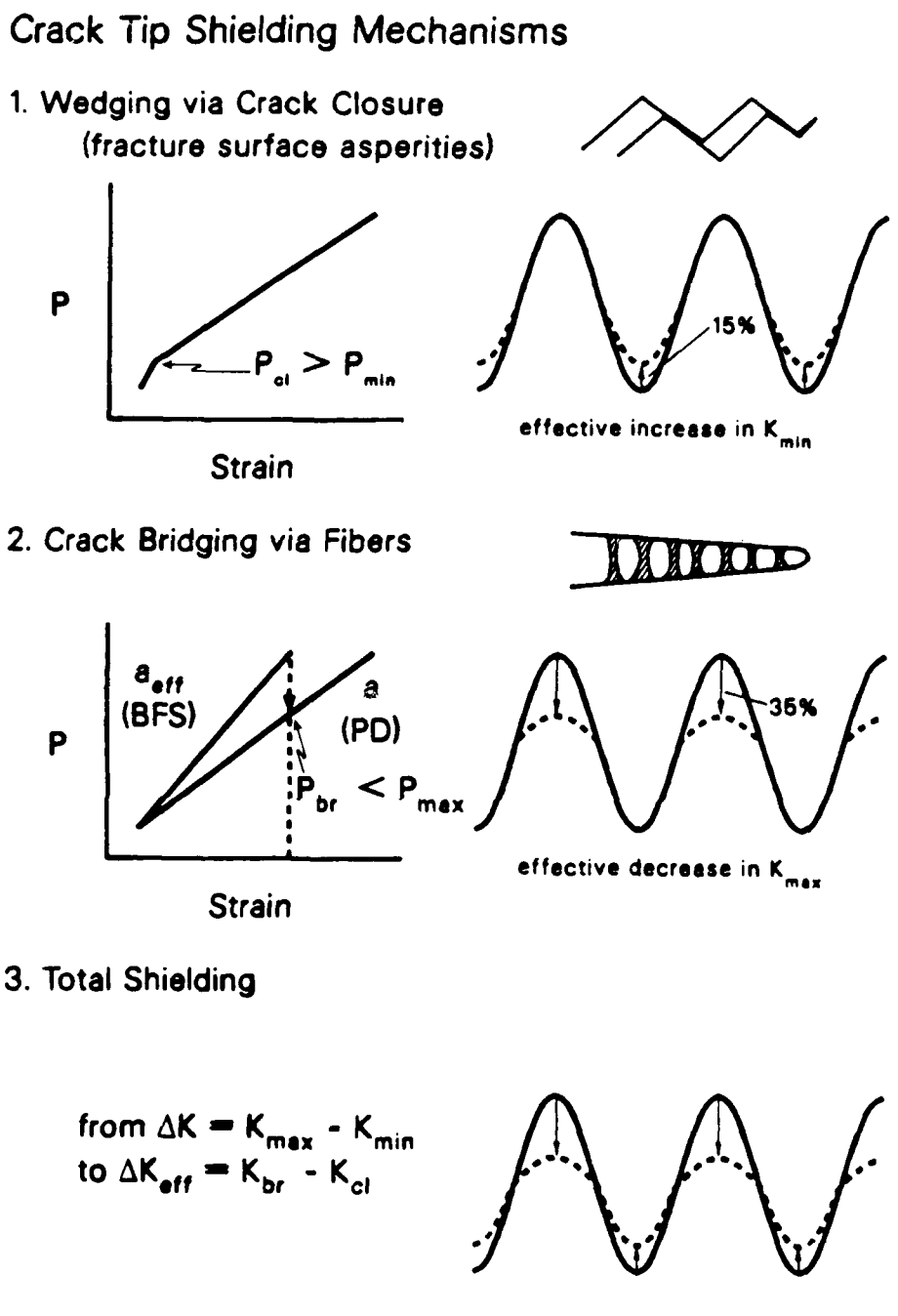


Fig. 2.11: Schematic illustrations of the primary crack-tip shielding mechanisms in ARALL, namely crack bridging and crack closure, and the experimental techniques used to quantify their effect on the effective near-tip "crack-driving force", i.e., $\Delta K_{eff} = K_{br} - K_{cl}$.

fracture-surface asperities (roughness-induced closure), aided by that induced by cyclic plasticity in the wake of the crack tip [e.g., refs. 30,34]. Accordingly, the closure stress intensity $K_{cl}$ is generally measured at the point of first contact of the crack surfaces during an unloading cycle [e.g., refs. 11,24]. In the present study, this was achieved by monitoring the elastic unloading compliance derived from the back-face strain gauge. Specifically, the data-acquisition and control system was programmed to determine, using a maximum correlation-coefficient procedure [11], the $K_{cl}$ value in real time in terms of the highest load where the elastic unloading compliance curve deviated from linearity (Fig. 2.11).

Using such procedures, closure levels in ARALL were found to be comparable with those in monolithic 2024-T351 sheet, but due to the higher $\Delta K$ levels required for propagation, their effect was proportionally smaller. In fact, closure was clearly of secondary importance to crack bridging in governing the value of $\Delta K_{eff}$ (see below). Specifically, closure levels were enhanced with decreasing $\Delta K$, as wedging is more effective at smaller crack opening displacements (CODs), but never resulted in more than a 15% increase in the effective $K_{min}$.

**Crack bridging:** The effect of crack bridging on the effective $K_{max}$ value was estimated using a new technique which combines measurement of the actual length of the full crack, using electrical-potential methods on the outer aluminum layer, with measurement of the

compliance of the bridged crack, using back-face strain gauges on the central aluminum layer (Fig. 2.4).

For each cycle, an elastic compliance curve of measured back-face strain vs. load P was determined; the slope of this curve (ignoring non-linearities due to closure at very low loads) represents the compliance of the bridged crack. Simultaneously, electrical-potential measurements were used to estimate the true length of the crack and, using an experimentally verified compliance calibration for back-face strain in the C(T) geometry [35-37], the theoretical compliance curve for the full-length (unbridged) crack was computed. As illustrated in Fig. 2.11, the slopes of these two curves are different. The experimental curve, derived from back-face strain measurements, is steeper (implying a smaller effective crack size) because the compliance is reduced by the fiber bridges; the theoretical curve, computed from electrical measurements of the true crack length, conversely is insensitive to the bridging effect.* Thus, at a given load, the measured strain (representative of the actual crack opening displacement) can be seen to be less than that predicted from the true (unbridged) crack length, because of the restraint on crack opening by the unbroken fibers. On this basis,

---

*In ARALL Laminates, the fiber bridges are non-conducting and thus do not compromise the electrical-potential measurements of true crack size. In materials where the bridges are conducting, or conversely where the matrix is non-conducting, actual crack size measurements can still made by monitoring the electrical resistance of a thin metal film, either evaporated or affixed to the side face of the specimen [e.g., refs. 38,39].

the reduction in effective $K_{max}$ due to bridging can be estimated by comparing these two curves at a given strain, for example, representative of the actual COD at maximum load. As shown in Fig. 2.11, the measured load ($P_{max}$) acting on the bridged crack length is clearly larger than that predicted ($P_{br}$) for the true (unbridged) crack length; the difference is essentially the load carried by the bridges. Accordingly, values of $P_{br}$ can be used to compute the approximate magnitude of $K_{br}$ as the effective maximum stress intensity in the fatigue cycle (after correcting for bridging).

With such procedures, the measured effect of crack bridging in ARALL was found to be far greater than that due to crack closure, resulting in up to 35% reductions in effective $K_{max}$ values in the fatigue cycle. The success of this approach may be judged with reference to Fig. 2.12 where, by using both closure and bridging corrections for shielding to compute $\Delta K_{eff}$ values from Eq. 2.1, the fatigue crack propagation data for ARALL-2 in the longitudinal (0°) orientation from Fig. 2.5, and from Fig. 2.10b for crack growth at constant $\Delta K$ from the wake-machined notch, are replotted in terms of $\Delta K_{eff}$. Once the allowance is made for both closure and bridging in the computation of the appropriate "crack driving force", crack propagation behavior in the laminate is no longer dependent upon history and crack size, and is a unique function of $\Delta K_{eff}$. (Results at the highest $\Delta K$ levels are not plotted in Fig. 2.12 as they involve

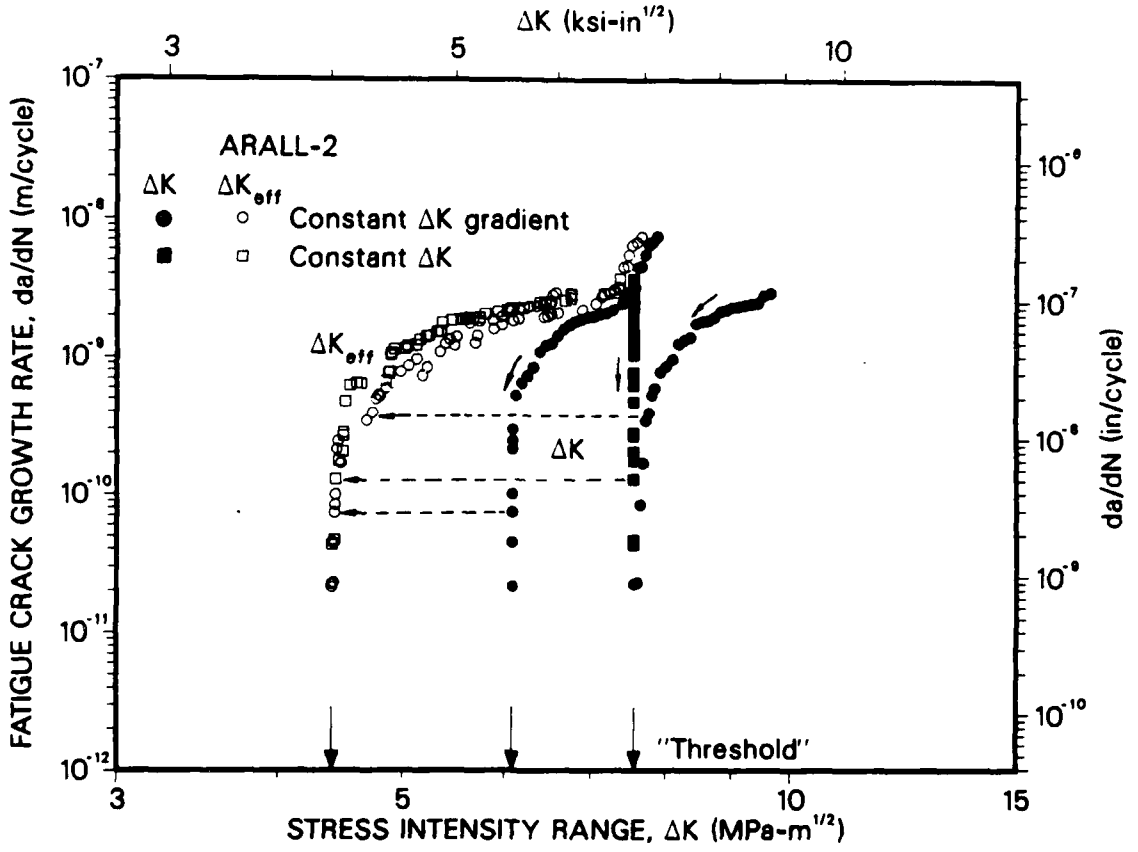


Fig. 2.12: Fatigue crack propagation results for ARALL-2 in the longitudinal (0°) orientation (from Figs. 2.5 and 2.10), plotted as a function of the nominal ($\Delta K = K_{max} - K_{min}$) and effective ($\Delta K_{eff} = K_{br} - K_{cl}$) stress-intensity ranges. Note how characterization in terms of $\Delta K_{eff}$ normalizes the previously crack-size and history dependent growth-rate data (horizontal dashed arrows). Small arrows on curves indicate whether data were obtained under decreasing or increasing growth-rate conditions.

macroscopic crack bifurcation and thus are not amenable to this simple analysis).

**Comparison with Advanced Aluminum Alloys:** From the perspective of high-performance applications, ARALL Laminates must compete with other advanced aluminum alloys, and in particular with aluminum-lithium alloys and metal-matrix composites. A comparison of the fatigue crack growth performance of these materials at ambient temperatures is shown in Fig. 2.13, based on the current ARALL-2 data and published results (at R = 0.1) for a commercial aluminum-lithium alloy 2090-T8E41 [40] and a SiC-particulate reinforced P/M Al-9%Zn-3%Mg-2½%Cu (ALCOA MB78) alloy [18]. The fatigue crack growth resistance of ARALL-2 in the transverse (90°) orientation is inferior to that of the other alloys; however, in the longitudinal (0°) orientation where cracks propagate perpendicular to the fiber direction, the laminate is superior to the metal-matrix composite, and furthermore shows significantly improved crack growth properties over the aluminum-lithium alloy. Since the 2090-T8E41 alloy may be considered as having (long-crack) fatigue properties superior to most, if not all, high-strength monolithic aluminum alloys [e.g., ref. 41], the use of ARALL for unidirectionally loaded, fatigue-critical structures provides a clear potential for markedly improved durability and damage-tolerance.

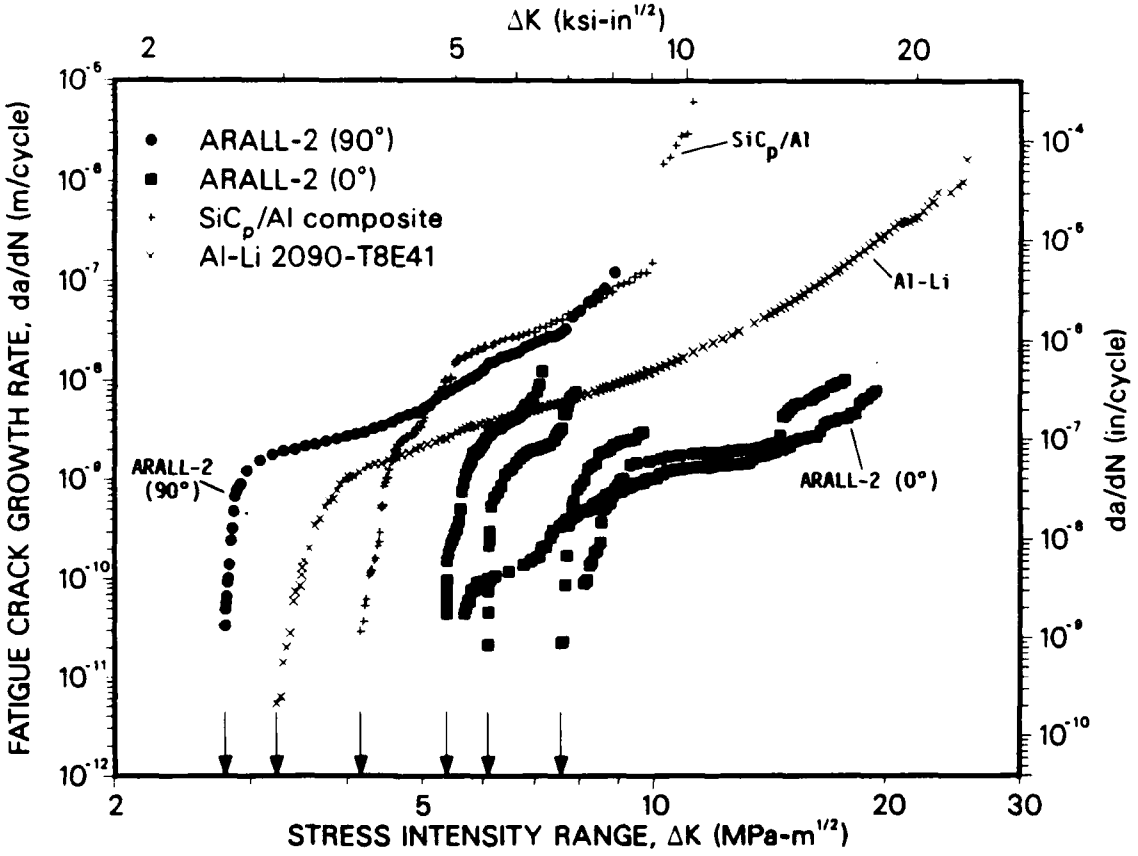


Fig. 2.13: Comparison of the fatigue crack propagation behavior of ARALL-2 (0° and 90° orientations), as a function of $\Delta K$ at $R = 0.1$, with other advanced aluminum alloys, namely aluminum-lithium alloy 2090-T8E41 and SiC-particulate reinforced P/M Al-9%Zn-3%Mg-2½%Cu (ALCOA MB78) metal-matrix composite. Data for 2090 and $SiC_p$/Al composite taken from refs. 30 and 18, respectively.

## 2.4 Conclusions

Based on an experimental study of fatigue crack propagation and crack-tip shielding behavior in a 2024-T351 aluminum-alloy/aramid-fiber epoxy 3/2 laminated composite, ARALL-2 Laminate, the following conclusions can be made:

1. Over the range of growth rates from $\sim 10^{-11}$ to $10^{-5}$ m/cycle (at R = 0.1), rates of fatigue crack propagation in ARALL-2 were found to be far slower than in the constituent matrix alloy 2024-T351 for crack advance perpendicular to the fiber direction (0° or longitudinal orientation); rates parallel to the fiber direction (90° or transverse orientation), conversely, were typically a factor of 4 faster.

2. Whereas differences in the growth-rate behavior between ARALL-2 and monolithic 2024-T351 can be predicted in the transverse (90°) orientation by assuming that the fibers play no role and that the aluminum-alloy layers carry all load, the superior crack-growth resistance of the laminate in the longitudinal (0°) orientation is associated with crack-tip shielding primarily by crack bridging from unbroken aramid fibers in the wake of the crack tip, with smaller contributions from crack closure and bifurcation.

3. The occurrence of crack bridging by unbroken fibers was promoted by controlled delamination, principally along the fiber/epoxy interfaces. Using wake-removal experiments, the length of crack over which the fibers remained unbroken in the wake of the crack tip, i.e., the bridging zone, was found to be between

3 to 5 mm, far larger than shielding zones measured for other mechanisms of shielding.

4. Owing to such extensive shielding from crack bridging, fatigue crack growth rates in the longitudinal (0°) orientation were crack-size and history dependent and showed no unique correlation with the applied stress-intensity range $\Delta K$.

5. A new experimental procedure, involving both electrical-potential and back-face strain compliance monitoring, is presented to enable the measurement of the reduction in effective $K_{max}$ in the fatigue cycle due to crack bridging. Coupled with standard unloading compliance measurements of the increase in effective $K_{min}$ due to crack closure, an effective (near-tip) stress-intensity range, $\Delta K_{eff}$, can be derived which embodies the effect of both crack bridging and closure. When characterized in terms of this local field parameter, longitudinal crack growth rates in ARALL lose their crack-size and history dependence and become a unique function of $\Delta K_{eff}$.

6. Under tension-tension fatigue loading, ARALL-2 Laminates display inferior crack-propagation resistance in the transverse (90°) orientation, and superior fatigue crack-propagation resistance in the longitudinal (0°) orientation, compared to monolithic aluminum and SiC-particulate reinforced aluminum alloys.

## 2.5 References


1. J. Schijve and L. B. Vogelesang, "Development of ARALL, a New Material for Aircraft Structures," Memorandum M-434, Delft Univ. of Technology, Dept. of Aerospace Engineering, Sept. 1982.

2. L. B. Vogelesang and J. W. Gunnink, "ARALL, a Material for the Next Generation of Aircraft. A State of Art," Report LR-400, Delft Univ. of Technology, Dept. of Aerospace Engineering, Aug. 1983.

3. L. N. Mueller, J. L. Prohaska, and J. W. Davis, in Proc. AIAA Aerospace Eng. Conf., AIAA, Los Angeles, CA, 1985.

4. L. B. Vogelesang and J. W. Gunnick, Materials and Design, 7 (1986) 2.

5. R. Marissen, Eng. Fract. Mech., 19 (1984) 261-277.

6. R. Marissen, K. H. Trautmann, J. Foth, and H. Nowack, in Fatigue 84, Proc. 2nd Intl. Conf. on Fatigue and Fatigue Thresholds, C. J. Beevers, ed., vol. II, EMAS Ltd., Warley, U.K., 1984, p. 1081.

7. R. Marissen, "Fatigue crack growth in Aramid Reinforced Aluminum Laminates (ARALL), Mechanisms and Predictions," Report DFVLR-FB-84-37, DFVLR, Istitut fur Werkstoff-Forschung, 1984.

8. R. Marissen, in Fatigue 87, Proc. 3rd Intl. Conf. on Fatigue and Fatigue Thresholds, R. O. Ritchie and E. A. Starke, eds., vol. 3, EMAS Ltd., Warley, U.K., 1987, p. 1271.

9. D. B. Marshall, B. N. Cox, and A. G. Evans, Acta Metall., 33 (1985) p. 2013.

10. R. J. Bucci, L. N. Mueller, R. W. Schultz, and J. L. Prohaska, in Advanced Materials Technology 87, Proc. 32nd Intl. SAMPE Symp., Sci. of Adv. Matls. and Proc. Eng., vol. 32, 1987, p. 902.

11. R. O. Ritchie and W. Yu, in Small Fatigue Cracks, R. O. Ritchie and J. Lankford, eds., TMS-AIME, Warrendale, PA, 1986, p. 167.

12. R. O. Ritchie, in Mechanical Behavior of Materials - V, Proc. 5th Intl. ICM Conf., M. G. Yan, S. H. Zhang, and Z. M. Zheng, eds., vol. 3, Pergamon Press, Oxford, U.K., 1987.

13. A. G. Evans, Z. B. Ahmad, D. G. Gilbert, and P. W. R. Beaumont, Acta Metall., 34 (1886) p. 79.

14. A. G. Evans and R. M. Cannon, Acta Metall., 34 (1986) p. 761.

15. A. G. Evans and K. T. Faber, J. Am. Ceram. Soc., 67 (1874) p. 250.

16. A. R. Rosenfield and B. S. Mujumdar, Metall. Trans. A, 18A (1987) p. 1053.

17. Y.-W. Mai and B. R. Lawn, J. Am. Ceram. Soc., 70 (1987) p. 289.

18. J.-K. Shang, W. Yu, and R. O. Ritchie, "Role of Silicon Carbide Particles in Fatigue Crack Growth in SiC Particulate-Reinforced Aluminum Alloy Composites," Mater. Sci. Eng. (1988), in press.

19. S. Suresh and R. O. Ritchie, in Fatigue Crack Growth Threshold Concepts, D. L. Davidson and S. Suresh, eds., TMS-AIME, Warrendale, PA, 1984, p. 227.

20. S. Suresh and R. O. Ritchie, Intl. Metals Rev., 29 (1981) p. 445.

21. J. Lankford, Fatigue Fract. Engng. Mater. Struct., 8 (1985) p. 161.

22. J. W. Hutchinson, Acta Metall., 35 (1987) p. 1065.

23. W. Elber, in Damage Tolerance in Aircraft Structures, ASTM STP 486, American Society for Testing and Materials, Philadelphia, PA, 1971, p. 230.

24. J. E. Allison, in Fracture Mechanics 18th Symposium, ASTM STP 945, R. P. Read and D. T. Reed, eds., American Society for Testing and Materials, Philadelphia, PA, 1987, p. 913.

25. M. A. Gregory, "ARALL 2 Laminates. Preliminary Technical Information," Alcoa Techical Report, Aluminum Company of America, Alcoa Center, PA, 1987.

26. R. J. Bucci, L. N. Mueller, L. B. Vogelesang, and and J. W. Gunnick, in Materials - Pathway to the Future, Proc. 33rd Intl. SAMPE Symp., Anaheim, CA, 1988; also Alcoa Technical Report No. 57-87-26, Alcoa, Alcoa Center, PA, 1987.

27. H. Tada, P. C. Paris, and G. R. Irwin, The Stress Analysis of Cracks Handbook (2nd edition), Paris Productions/Del Research Corp., St. Louis, MO, 1985.

28. F. E. H. M. Smulders and G. H. J. J. Roebroeks, "Mechanism of Prepreg Failure under R = 0 Fatigue Loading in ARALL Laminate," Technical report, Delft University of Technology, Dept. of Aerospace Engineering, 1987.

29. K. Minakawa, J. C. Newman, and A. J. McEvily, Fatigue Engng. Mater. Struct., 6 (1983) p. 359.

30. E. Zaiken and R. O. Ritchie, Metall. Trans. A, 16A (1985) p. 1467.

31. S. Suresh, D. M. Parks, and R. O. Ritchie, in Fatigue Thresholds, Proc. 1st Intl. Conf. on Fatigue Thresholds J. Bäcklund, A. F. Blom, and C. J. Beevers, eds., vol. I, EMAS Ltd., Warley, U.K., 1982 p. 391.

32. S. Suresh and R. O. Ritchie, Scripta Metall., 17 (1983) p. 575.

33. J.-L. Tzou, C. H. Hseuh, A. G. Evans, and R. O. Ritchie, Acta Metall., 33 (1985) p. 117.

34. R. D. Carter, E. W. Lee, E. A. Starke, and C. J. Beevers, Metall. Trans. A, 15A (1984) p. 555.

35. W. F. Deans and C. E. Richards, J. Test. Eval., 7 (1979) p. 147.

36. C. E. Richards and W. F. Deans, in The Measurement of Crack Length and Shape during Fracture and Fatigue, C. J. Beevers, ed., EMAS Ltd., Warley, U.K., 1980, p. 28.

37. D. C. Maxwell, "Strain-Based Compliance Method for Determining Crack Length for a C(T) Specimen," Materials Laboratory, Air Force Wright Aeronautical Laboratories, Report No. AFWAL-TR-87-4046, Wright-Patterson Air Force Base, Dayton, OH, 1987.

38. P. K. Liaw, H. R. Hartmann, and W. A. Logsdon, J. Test. Eval., 11 (1983) p. 202.

39. R. H. Dauskardt, W. Yu, and R. O. Ritchie, J. Am. Ceram. Soc., 70 (1887) p. C248.

40. K. T. Venkateswara Rao, W. Yu, and R. O. Ritchie, Metall. Trans. A, 19A (1988) p. 549.

41. K. T. Venkateswara Rao, W. Yu, and R. O. Ritchie, "On the Behavior of Small Fatigue Cracks in Commercial Aluminum-Lithium Alloys," Eng. Fract. Mech. (1988) in press.

# 3. FATIGUE-CRACK PROPAGATION STUDIES IN CONTINUOUSLY-REINFORCED METAL-MATRIX COMPOSITES

## 3.1 Studies in SiC-Fiber-Reinforced Aluminum Alloys

The focus of this project is to investigate the mechanisms affecting fatigue-crack growth and crack-tip shielding in continuously-reinforced metal-matrix composites, specifically with 40% unidirectional SC5-8 (SiC) fibers in a 6061 aluminum-alloy matrix. The composites, which were supplied by Lockheed, were fabricated from 8 layers of 140-μm-diameter fibers, plasma sprayed with 6061 and diffusion bonded together. The resulting 1.5 mm-thick sheet was annealed for 2 hr at 430°C, and slow cooled at 30°C/hr to 100°C. Preliminary measurements indicate an elastic modulus of 240 GPa in the 0° orientation, and 90 GPa in the 90° orientation, representing, respectively, a factor of $\sim$3.5 and 1.3 improvement over the unreinforced alloy.

Initial tests are directed at characterizing the long (> 5 mm) crack and microstructurally-small (1 to 500 μm) crack growth-rate behavior as a function of orientation, i.e., along the fiber direction (90° orientation), perpendicular to the fiber direction (0° orientation), and in the 45° orientation. Long-crack tests are being performed on compact C(T) and center-cracked tension CC(T) specimens at a range of load ratios to assess the varying degrees of crack deflection, crack closure and bridging in the two geometries; small-crack tests, conversely, are being performed on unnotched cantilever-

beam bending samples, where the initiation and early growth of naturally-occurring cracks is monitored by periodic replication.

Results to date on the long-crack experiments at R = 0.1 on the compact geometry have shown substantial crack deflection and crack bifurcation in the 0° orientation. In the 90° orientation, conversely, fatigue cracks were observed to follow the aluminum matrix and Al/fiber interfaces, with rare instances of fiber breakage. Premature arrests, i.e., apparent fatigue thresholds, were frequently seen, apparently due to encounters between the crack and the fiber surface. Using a series of sequential load-shedding schemes, a lower-bound fatigue threshold of approximately 5.5 MPa$\sqrt{m}$ was determined.

### 3.2 Studies on Graphite-Fiber Reinforced Magnesium Alloys

Similar studies are in progress on a magnesium alloy continuously reinforced with 20% unidirectional graphite fibers, which was manufactured by DWA Composite Specialties Inc. The particular panel under study consists of eight unidirectional graphite-fiber layers (P75) fused together with a magnesium matrix; the surfaces are protected by an 0.025-mm-thick titanium cladding. The total panel thickness is 0.78 mm. A three-dimensional optical micrograph of the microstructure is shown in Fig. 3.1.

Due to the limited amount of material available, miniature compact C(T) specimens, of 20.3 mm width, were used to determine the fatigue and fracture properties. For crack extension parallel to the

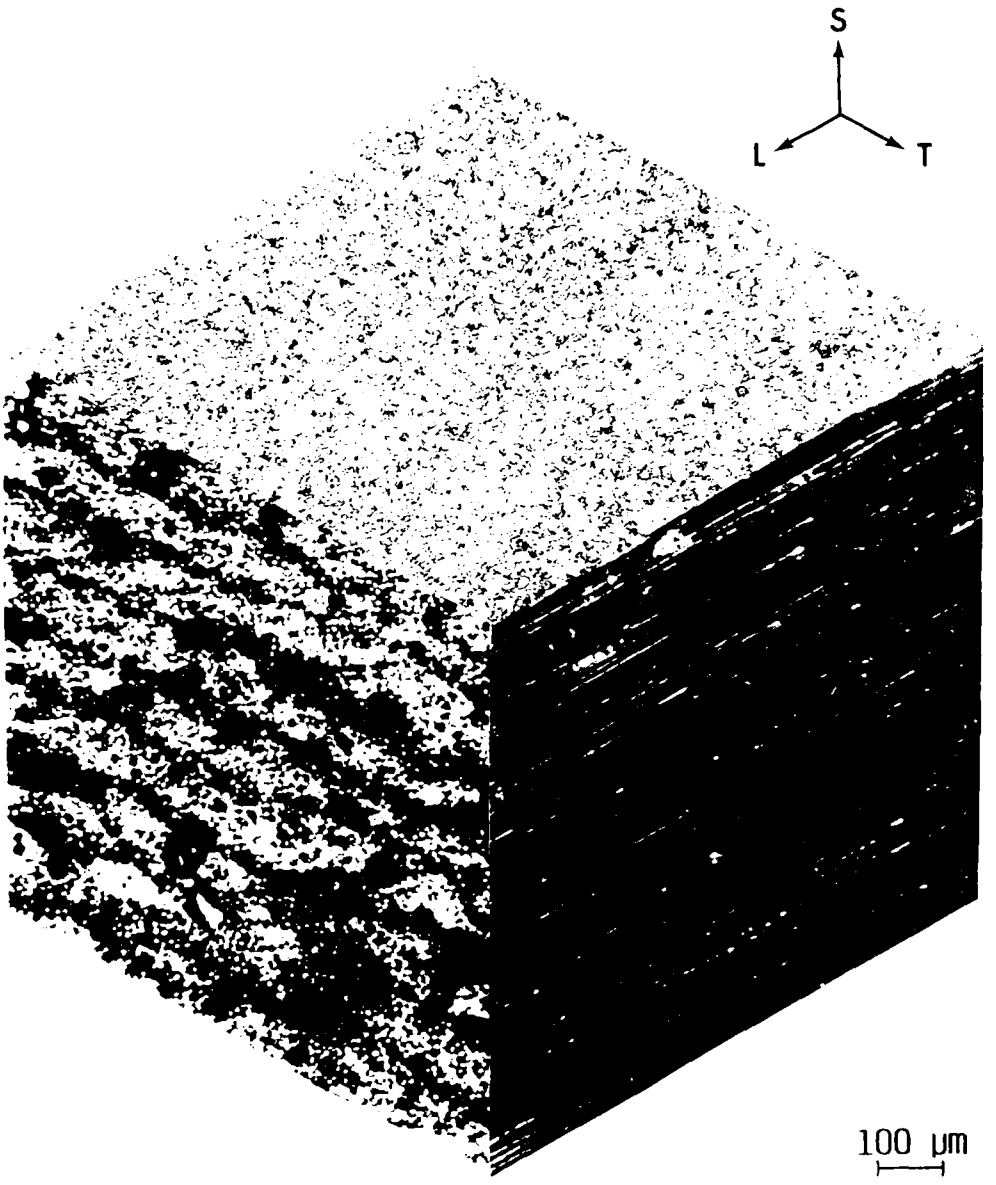


Fig. 3.1: Three-dimensional optical micrograph of the magnesium alloy continuously reinforced with unidirectional graphite fibers.

fiber direction (0° orientation), crack-growth behavior was confined to the fiber/matrix interface, similar to results for ARALL-2 laminates and the SiC-continuously-reinforced aluminum alloy (sections 2 and 3.1, respectively). Moreover, extensive delamination and debonding between matrix and fiber, leading to crack bifurcation, were observed for crack growth perpendicular to the fiber direction (90° orientation).

To examine the potential for crack deflection and bifurcation in these composites, similar to studies in the SiC-reinforced aluminum, tests will be additionally performed in a geometry where off-angle cracking is less stabilized. Accordingly, miniature center-cracked tension CC(T) samples are being machined to compare with the compact results.

## 4. BRIEF SUMMARY OF FUTURE WORK

In the coming year, studies on ARALL Laminates will be extended to higher-temperature versions, specifically ARALL-4 which is based on 2024-T8 alloy with a higher-temperature cure (350°F) prepreg, and to pre-stretched versions, specifically ARALL-1 based on 7075-T6 alloy. In view of the tendency for crack deflection in certain orientations, experiments will be additionally performed in center-cracked sheet CC(T) geometries, to compare with the current compact-geometry C(T) tests; it is reasoned that since off-angle cracks will not be stabilized, far less deflection will occur in the CC(T) tests with the result that growth rates may be significantly faster.

Additionally, emphasis will be placed on variable-amplitude tests where it is expected that the laminates will not experience the same degree of post-overload retardations as monolithic alloys because of the failure of fibers during the overload cycles; i.e., crack bridging will be diminished.

Studies in the continuously-reinforced aluminum and magnesium alloys will be directed at ellucidating the prevalent crack-growth and shielding mechanisms. In view of the paucity of experimental data, testing will be directed at a comparison of long (> 5 mm) and microstructurally-small (1 to 500 μm) crack-growth behavior, performed as a function of specimen orientation with respect to the fiber axis.

## 5. ACKNOWLEDGEMENTS

This work was supported by the U.S. Air Force Office of Scientific Research under Grant No. AFOSR-87-0158, with Dr. A. H. Rosenstein as contract monitor. The authors would like to thank Alcoa, specifically Drs. R. J. Bucci and L. N. Bueller, for supplying the ARALL Laminate materials, the Lockheed Palo Alto Research Laboratories, specifically Drs. T. G. Nieh and J. Wadsworth, for supplying the SiC-fiber continuously-reinforced aluminum-alloy sheet, and Dr. S. Fishman of ONR for supplying the graphite-reinforced magnesium alloy.

## 6. PROGRAM ORGANIZATION AND PERSONNEL

The work described was performed in the Department of Materials Science and Mineral Engineering, University of California in Berkeley, under the supervision of Dr. R. O. Ritchie, Professor of Materials Science, aided by a research engineer, graduate student research assistants and undergraduate research helpers. The individual personnel are listed below:

i) Professor R. O. Ritchie, Principal Investigator
(Department of Materials Science and Mineral Engineering)

ii) Dr. W. Yu, Assistant Research Engineer
(Department of Materials Science and Mineral Engineering)

iii) S. C. Siu, Graduate Student Research Assistant
(Department of Materials Science and Mineral Engineering)

iv) A. Nguyen, Undergraduate Engineering Aide
(Department of Materials Science and Mineral Engineering)

## 7. PUBLICATIONS

### 7.1 Refereed Journals

1. R. O. Ritchie, W. Yu and R. J. Bucci: "Fatigue Crack Propagation in ARALL Laminates: Measurement of the Effect of Crack-Tip Shielding from Crack Bridging," Engineering Fracture Mechanics, 1988, in press.

### 7.2 Invited Presentations

2. R. O. Ritchie: "Fatigue and Fracture Mechanics of Advanced Materials," invited seminar to Grumman Aerospace Co., Plainview, NY, Sept. 1987.

3. R. O. Ritchie: "Threshold Fatigue Behavior of Long and Short Cracks," invited presentation to ASM Symp. on Fracture, at the ASM Materials Congress, Cincinnati, OH, Oct. 1987.

4. R. O. Ritchie: "Fatigue-Crack Propagation in ARALL Laminates: Models and Experiments," presented at Alcoa Conference on ARALL Laminates, Seven Springs, PA, Oct. 1987.

5. R. O. Ritchie: "Ductile-Matrix Composites: Fracture and Fatigue," invited presentation at the 1988 Annual Winter Workshop on Composite Materials, University of California, Santa Barbara, Ca, Jan. 1988.

6. R. O. Ritchie: "Toughening Mechanisms in Composite Materials," invited keynote lecture, Topical Symp. on Micromechanisms of Fracture in Metal Matrix Composites, 117th TMS Annual Meeting, Phoenix, AZ, Jan. 1988.

7. W. Yu and R. O. Ritchie: "Measurement of Crack Bridging during Fatigue Propagation in Laminate Composites," invited presentation to ASTM Committee E9-01 on Fatigue Research, ASTM Spring Meeting, Sparks, NV, April 1988.

## 8. DISTRIBUTION LIST

AFOSR/NE
ATTN: Dr. A. H. Rosenstein
Bldg. #410
Bolling Air Force Base
Washington, D.C. 20332

AFWAL/MLLM
ATTN: Branch Chief
Wright-Patterson Air Force Base
Dayton, OH 45433

AFWAL/MLLS
ATTN: Branch Chief
Wright-Patterson Air Force Base
Dayton, OH 45433

AFWAL/MLLN
ATTN: Branch Chief
Wright-Patterson Air Force Base
Dayton, OH 45433

Dr. Hugh R. Gray
NASA Lewis Research Center
Materials and Structures Division
21000 Brookpark Rd.
Cleveland, OH 44135

Drs. R. J. Bucci, O. Richmond, W. H. Hunt,
L. N. Mueller, and J. T. Staley
Alcoa Technical Center
Alcoa Laboratories
Alcoa Center, PA 15069

Drs. T. G. Nieh and J. Wadsworth
Lockheed Palo Alto Research Laboratories
0/93-10B/204
3251 Hanover St.
Palo Alto, CA 94304-1191

END

DATE

FILMED

DTIC

9-88